

TOPICAL REVIEW • OPEN ACCESS

Atomic-scale engineering of advanced catalytic and energy materials via atomic layer deposition for eco-friendly vehicles

To cite this article: Xiao Liu *et al* 2023 *Int. J. Extrem. Manuf.* **5** 022005

View the [article online](#) for updates and enhancements.

You may also like

- [Progresses on cryo-tribology: lubrication mechanisms, detection methods and applications](#)
Wenyan Cui, Hongzhan Chen, Jianxun Zhao *et al.*
- [Electrostatic atomization minimum quantity lubrication machining: from mechanism to application](#)
Wenhao Xu, Changhe Li, Yanbin Zhang *et al.*
- [Advances in micro cutting tool design and fabrication](#)
John O'Hara and Fengzhou Fang

Topical Review

Atomic-scale engineering of advanced catalytic and energy materials via atomic layer deposition for eco-friendly vehicles

Xiao Liu, Yu Su and Rong Chen* 

State Key Laboratory of Intelligent Manufacturing Equipment and Technology, School of Mechanical Science and Engineering, Huazhong University of Science and Technology, 1037, Luoyu Road, Wuhan, Hubei, People's Republic of China

E-mail: rongchen@mail.hust.edu.cn

Received 16 November 2022, revised 31 January 2023

Accepted for publication 22 March 2023

Published 11 April 2023



CrossMark

Abstract

Zero-emission eco-friendly vehicles with partly or fully electric powertrains have exhibited rapidly increased demand for reducing the emissions of air pollutants and improving the energy efficiency. Advanced catalytic and energy materials are essential as the significant portions in the key technologies of eco-friendly vehicles, such as the exhaust emission control system, power lithium ion battery and hydrogen fuel cell. Precise synthesis and surface modification of the functional materials and electrodes are required to satisfy the efficient surface and interface catalysis, as well as rapid electron/ion transport. Atomic layer deposition (ALD), an atomic and close-to-atomic scale manufacturing method, shows unique characteristics of precise thickness control, uniformity and conformality for film deposition, which has emerged as an important technique to design and engineer advanced catalytic and energy materials. This review has summarized recent process of ALD on the controllable preparation and modification of metal and oxide catalysts, as well as lithium ion battery and fuel cell electrodes. The enhanced catalytic and electrochemical performances are discussed with the unique nanostructures prepared by ALD. Recent works on ALD reactors for mass production are highlighted. The challenges involved in the research and development of ALD on the future practical applications are presented, including precursor and deposition process investigation, practical device performance evaluation, large-scale and efficient production, etc.

Keywords: atomic layer deposition, eco-friendly vehicle, exhaust gas catalysis, lithium ion battery, hydrogen fuel cell

* Author to whom any correspondence should be addressed.



Original content from this work may be used under the terms of the [Creative Commons Attribution 4.0 licence](https://creativecommons.org/licenses/by/4.0/). Any further distribution of this work must maintain attribution to the author(s) and the title of the work, journal citation and DOI.

1. Introduction

Eco-friendly vehicles are the sustainable future of vehicle industry by reducing the emissions of air pollutants and improving the energy efficiency, which are powered by advanced engine technologies with matched zero-emission control system or partly and fully powered by clean energy technologies, such as battery and fuel cell [1–5]. Nowadays the sales of electric vehicles have grown year by year, yet the continuous efforts will be made to develop efficient catalysts for exhaust emission control in the coming decades, as internal combustion engines are still widely used in fossil fuel vehicles and transitional hybrid electric vehicles [6]. Both lithium-ion battery and hydrogen fuel cell are impressive power supplies for electric vehicles. Owing to the increasing specific energy and decreasing cost in the past decades, lithium-ion battery with lightweight, compactness and affordability has almost exclusively powered commercial electric vehicles at present [7, 8]. Different from lithium-ion battery, hydrogen fuel cell produces electricity from the electrochemical oxidation of hydrogen [9]. Since the first commercialization of hydrogen fuel cell vehicle in 2014 by Toyota, much attention has been paid to overcoming the technical barriers for large scale applications, such as cost, performance and durability [10].

Advanced catalytic and energy materials are essential for the key components of eco-friendly vehicles, such as exhaust emission control system, lithium ion battery and hydrogen fuel cell. Although the roles of these materials are different in the components, improving the performance of catalysis and electron/ion transport is important for development of advanced catalytic and energy materials. As shown in figure 1, precious metals or metal oxides are commonly applied as exhaust catalysts to eliminate carbon monoxide (CO), hydrocarbons, nitrogen oxides (NO_x) and particulate matter. These catalytic reactions at gas/solid two-phase interfaces are sensitive to the surface and interface structures of exhaust catalysts [11, 12]. As an energy conversion component, hydrogen fuel cell involves the electrochemical catalysis at gas/solid/liquid three-phase interfaces, which also needs highly efficient catalysts to accelerate the sluggish kinetics of catalytic reactions on electrodes [13, 14]. Moreover, the stability of exhaust gas catalysts and hydrogen fuel cell catalysts has also attracted much attention, which is closely related to their nanostructures [15]. Furthermore, the electron/ion transport is important for energy storage and conversion for both lithium-ion battery and hydrogen fuel cell. For instance, the high energy density of lithium-ion battery usually brings out the problems of low cycle life and poor safety that requires surface modifications of cathode and anode materials to improve their stability and simultaneously ensure electron/ion transport [16, 17]. The transport of electron/ion and reactants in the membrane electrode assembly (MEA) can affect the power density and efficiency of hydrogen fuel cell, which requires the precise control and modification of electrochemical interfaces [18, 19]. Overall, the precise control of surface and interfacial structure of catalytic and energy material is of great significance to satisfy the highly efficient surface and interface catalysis, as well as rapid electron/ion transport.

Atomic layer deposition (ALD), an atomic and close-to-atomic scale manufacturing method, is capable of designing and engineering advanced catalysts and electrodes, which exhibits higher accuracy than conventional wet-chemistry methods [20]. As shown in figure 1, ALD is a thin film technology based on alternately self-limited saturated adsorption and chemical reaction of gas-phase precursors on substrate surface, which is firstly invented by Tuomo Suntola in 1970s [21]. In a typical ALD cycle, an inert gas is introduced to purge out unreacted precursor A or B to separate two self-limited chemical reactions on substrate. The self-limited chemical reactions between precursors and substrate result in the superior capability of ALD for preparing uniform and conformal films on substrate with high aspect ratio micro-nano structures. The thickness of films prepared by ALD can also be precisely controlled by tuning the ALD cycles. ALD has achieved industrial applications in displays, microelectronics and solar energy with its unique characteristics of precise thickness control, uniformity and conformality [22–24]. For vehicles, ALD has been performed to prepare precious metal or metal oxide nano coatings to improve the performance of micro-electro-mechanical system, such as capacitive sensor, micro-resonator and high-power radar [25–27]. The structure components can be modified by ALD coatings to increase the mechanic strength and corrosion resistance [28–31]. As a promising energy storage device, supercapacitor also requires surface modification on the electrodes to increase the energy density and cyclic stability. ALD technique has not only been utilized to coat active materials on high-surface-area supports to improve the energy density, but also played an important role in preparing passivation layer to enhance electrochemical stability and minimize self-discharge [32–35]. Moreover, ALD is also considered as a thin-film micromanufacturing technique for designing and preparing microbatteries and electrochemical energy storage devices [36, 37].

Indeed, applications of ALD for catalysts, batteries and fuel cells have also attracted widespread attention to the enhancement of their chemical and electrochemical performance [38, 39]. Since the catalysts for exhaust gas cleaning and energy conversion in fuel cells, as well as electrode materials in batteries are powder materials with high specific surface areas, the ALD modifications on these catalytic and energy materials suffer from agglomeration problem and usually exhibit lower efficiency than that of conventional ALD on planer substrates. In order to achieve efficient and uniform gas-solid contact between precursors and particles, continuous fluidization or mechanical agitation of particle bed has been introduced into the special reactors for ALD on porous materials [40–42]. The ALD processes for surface modifications on powder materials have also been summarized in previously reported reviews [43–46]. Since the invention of ALD in 1970s, it has been applied to prepare supported heterogeneous catalysts [47]. In the past decade, advanced catalysts with atomically precise control over the active sites and composite structures have been designed and prepared by ALD, such as supported uniform metal particles, clusters and single atoms, as well as various unique overcoating structures, which exhibit enhanced activity, selectivity and stability for a variety

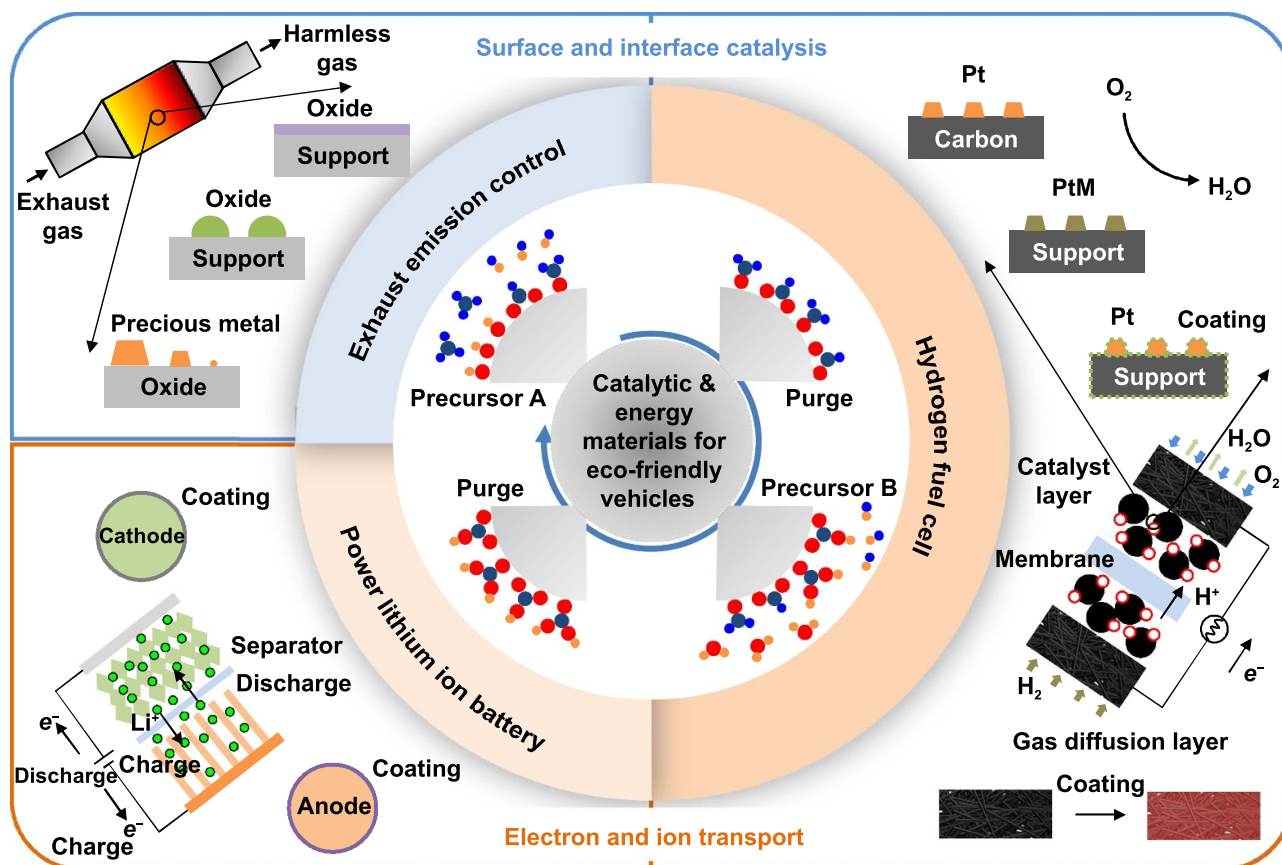


Figure 1. Schematic diagram of the general ALD process based on binary reaction sequence and the applications for synthesis and surface modification of advanced catalytic and energy materials in eco-friendly vehicles.

of catalytic reactions [48, 49]. Since the early work of ALD coating on LiCoO_2 cathodes to improve the durability, ALD is proposed to modify the surface and interface of electrode materials and separators for batteries and fuel cells, which can result in the improvements of structural and chemical stability, electronic and ionic conductivity, as well as mass transport for energy storage and conversion [32, 50–52]. Overall, ALD has emerged as an important technique for the surface and interface engineering of advanced catalytic and energy materials, which is of significance for the research and development for eco-friendly vehicles.

In this review, the ALD processes on materials for catalysis and energy, as well as their enhanced performance for exhaust emission control, power lithium ion battery and hydrogen fuel cell are comprehensively introduced. In the following sections, the catalysts such as precious metal, non-precious metal and oxide prepared by ALD for exhaust emission control are reviewed initially. Then, an overview of ALD for the surface and interface modification of lithium ion battery materials, such as cathode, anode and separator is provided. As a controllable preparation and modifications methods for catalysts and electrodes, ALD processes applied for hydrogen fuel cell are reviewed. At the end of this review, the ALD reactors for mass production are introduced, while the challenges involved in the research and development of ALD

on the future practical applications in eco-friendly vehicles are discussed.

2. Catalysts for exhaust emission control

In order to satisfy the current near-zero vehicle emission regulations for vehicle exhaust pollutants, such as CO, hydrocarbons, NO_x and particulate matter, the activity of catalyst at low temperature is the key to eliminate the exhaust pollutants at cold start stage, while the high temperature stability determines the lifetime of catalyst at working conditions. Since the catalytic reactions of exhaust pollutants occur on the surface of catalysts, the catalytic activities are sensitive to the atomic structures of surface and interface of exhaust catalysts. Table 1 has summarized the recently reported catalysts prepared by ALD for exhaust emission control. Supported Pt group metal catalysts are commonly used as the three-way catalyst and diesel oxide catalyst for gasoline and diesel aftertreatment, respectively. Composite catalysts with smaller precious metal size and stronger metal-support interaction have been prepared to improve the low temperature activity. A promising strategy has emerged to encapsulate Pt-based nanoparticles in a protective layer to enhance the high temperature stability. Supported non-precious metal or oxide

Table 1. Summary of catalysts prepared by ALD for exhaust emission control.

Type of catalyst	Catalyst	ALD material	Optimal cycles and thickness/size	Catalytic reaction	Catalytic performance	References
Supported Pt group metal catalyst	Pt ₁ /CeO ₂	Pt	1 cycle, single atom	CO oxidation	T_{100} : 98 °C; activation energy: 0.41 eV (test with the presence of water)	[53]
	1.2%Pt ₁ /D-CeO ₂	Pt	1 cycle, single atom	CO oxidation	T_{50} : 192 °C (T_{50} decreases to 175 °C with the presence of water)	[54]
	Pt _n /CeCuO ₂	Pt	1 cycle, 0.75 nm	CO oxidation	T_{onset} : 8 °C; activation energy: 39.49 kJ mol ⁻¹ ; TOF at 80 °C: 0.26 s ⁻¹	[55]
	Pt/TiO ₂	Pt	0.95 nm	Diesel oxidation catalysis	T_{50} of CO and hydrocarbon: 224 and 285 °C	[56]
	Pt/CeO ₂	Pt	40 cycles, 3.77 nm	Diesel oxidation catalysis	T_{90} of CO and hydrocarbon: ~180 °C	[57]
	Pt/SiO ₂	Pt	5 cycles, 1.9 nm	CO oxidation	T_{100} : 180 °C; TOF at 200 °C: 1.8 s ⁻¹	[58]
	Pt/SrTiO ₃	Pt	5 cycles, 3–4 nm	Propane oxidation	T_{50} : 168 °C; TOF: ~2.07 s ⁻¹	[59]
	Pd/SrTiO ₃ nanocuboids	Pd	1 cycle, 1.7 nm	CO oxidation	Activation energy: 76.3 kJ mol ⁻¹ ; TOF at 80 °C: 0.0029 s ⁻¹	[60]
	Pt/SmMn ₂ O ₅	Pt	1 cycle, 0.5–0.9 nm	CO oxidation	T_{50} : 86 °C; activation energy: 43.87 kJ mol ⁻¹ ; TOF at 90 °C: 0.033 s ⁻¹	[61]
	Pd/SnO ₂ /h-BN	Pd SnO ₂	4 cycles, / 50 cycles, 4.5 nm	CO oxidation	T_{100} : 186 °C; TOF at 140 °C: ~0.02 s ⁻¹	[62]
	Pd/CeO ₂ /Al ₂ O ₃	CeO ₂	20 cycles, 0.4 nm	CO oxidation	T_{10} : ~67 °C (after calcination at 800 °C)	[63]
	Pd/CeO ₂ /Al ₂ O ₃	Pd CeO ₂	1 cycle, / 20 cycles, ~0.4 nm	CO oxidation	Activation energy: 50 kJ mol ⁻¹ ; TOF at 150 °C: 31 s ⁻¹	[64]
	Pd/Co ₃ O ₄ /Al ₂ O ₃	Pd Co ₃ O ₄	1 cycle, / 30 cycles, ~0.04 nm	CH ₄ oxidation	TOF at 300 °C: 4.5 s ⁻¹	[64]
	Pd/Ce _{0.5} Zr _{0.5} O ₂ /Al ₂ O ₃	Ce _{0.5} Zr _{0.5} O ₂	50 cycles, ~1.0 nm	CO oxidation	T_{10} : 80 °C	[65]
	Pt/LaFeO ₃ /MgAl ₂ O ₄	Pt LaFeO ₃	1 cycle, 1–2 nm ~32 cycles, ~0.56 nm	CO oxidation	T_{50} : ~177 °C; Activation energy: 60 kJ mol ⁻¹	[66]
	Pt/CaTiO ₃ /MgAl ₂ O ₄	Pt CaTiO ₃	1 cycle, / ~50 cycles, 1 nm	CO oxidation	T_{50} : ~277 °C	[67]
Pt/LaCoO ₃ /MgAl ₂ O ₄	Pt LaCoO ₃	1 cycle, / 30 cycles, 0.5 nm	CO oxidation	T_{50} : ~137 °C	[68]	
Pd/LaFeO ₃ /MgAl ₂ O ₄	LaFeO ₃	60 cycles, 1.2 nm	CH ₄ oxidation	Activation energy: 75 kJ mol ⁻¹	[69]	
Encapsulated Pt group metal catalyst	Al ₂ O ₃ /Pd/SiO ₂	Al ₂ O ₃	40 cycles, 8 nm	CH ₄ oxidation	T_{50} : ~340 °C	[70]
	Al ₂ O ₃ /Pd/Al ₂ O ₃	Al ₂ O ₃	45 cycles, /	CH ₄ oxidation	T_{50} : 391 °C	[71]
	Al ₂ O ₃ /Pt/SiO ₂	Pt Alucone	5 cycles, 1.7 nm 20 cycles, 2 nm	CO oxidation	T_{100} : 210 °C	[72]
	ZrO ₂ /Pd/Al ₂ O ₃	ZrO ₂	50 cycles, 1 nm	CH ₄ oxidation	Reaction rate at 212 °C: 10 ¹⁹ CH ₄ s ⁻¹ g _{Pd} ⁻¹	[73]
	ZrO ₂ /Pd/CeO ₂	ZrO ₂	20 cycles, 0.4 nm	CH ₄ oxidation	Activation energy: 65 kJ mol ⁻¹	[74]
	MnO _x /Pt/Al ₂ O ₃	Pt MnO _x	/, 3 nm 50 cycles, 0.83 nm	CO oxidation	Activation energy: 70 kJ mol ⁻¹	[75]

(Continued.)

Table 1. (Continued.)

Supported metal or oxide catalyst	Co ₃ O ₄ /Pt/Al ₂ O ₃	Pt Co ₃ O ₄	2 cycles, 2 nm 50 cycles, 1.7 nm	CO oxidation	T_{50} : 70 °C; activation energy: 22.17 kJ mol ⁻¹ , TOF at 60 °C: 0.027 s ⁻¹	[76]
	Pt/CeO _x	Pt CeO _x	20 cycles, 2.3 nm 100 cycles, 1.8 nm	CO oxidation	T_{50} : 200 °C; activation energy: 71.5 kJ mol ⁻¹	[77]
	NiO _x /Pt/Al ₂ O ₃	Pt NiO _x	20 cycles, 1.44 nm 10 cycles, /	CO oxidation	T_{50} : 184 °C; activation energy: 88.79 kJ mol ⁻¹	[78]
	Fe/SiO ₂	Fe	25 cycles, single atom	CO oxidation	T_{100} : 410 °C; TOF at 360 °C: ~0.011 s ⁻¹	[79]
	NiO/Al ₂ O ₃	NiO	50 cycles, ~1 nm	CO oxidation	TOF at 30 °C: 1.1 × 10 ⁻⁴ s ⁻¹	[80]
	8cZr/8cCe-Cu/ZSM-5	ZrO ₂ CeO ₂	8 cycles, / 8 cycles, /	SCR of NO _x	NO _x conversion at 350 °C: ~40%	[81]
	VO _x /TiO ₂ /SBA-15	TiO ₂ VO _x	3 cycles, / 3 cycles, /	SCR of NO _x	NO _x conversion at 250 °C: 61.1%; N ₂ selectivity at 250 °C: 98.1%	[82]
	MnO ₂ -graphene oxide-TiO ₂	TiO ₂	4 cycles, /	SCR of NO _x	Temperature range for NO conversion above 85%: 150-280 °C	[83]
	Cu-SSZ-13@SiO ₂	SiO ₂	40 cycles, 10 nm	SCR of NO _x	Temperature range for NO _x conversion above 90%: 180-470 °C; N ₂ selectivity: >97.8%	[84]
	Fe ₂ O ₃ @CeO ₂ /TiO ₂	Fe ₂ O ₃	30 cycles, /	SCR of NO _x	NO _x conversion at 250 °C: ~78%	[85]
	CeO ₂	CeO ₂	2000 cycles, 76 nm	Soot combustion	Complete soot conversion temperature: 450 °C	[86]
	Ag doped CeO ₂	CeO ₂ Ag	1500 cycles, / 150 cycles, /	Soot combustion	Complete soot conversion temperature: 390 °C	[87]

catalysts have been prepared by ALD for SCR of NO_x and soot combustion.

2.1. Supported Pt group metal catalysts

By utilizing the initial island nucleation stage of metal ALD, ALD has been applied to prepare metallic nanoparticles for catalysis [48, 88]. Since the self-limiting chemical reactions of sequential precursors on the surface of supports, ALD provides the opportunity to deposit uniform metal nanoparticles with precisely controlled size, while the mass loading of metal is affected by the nature of metal precursors, deposition temperature and surface structures of supports. As another factor to affect the catalytic activity, the density of metal particles is also closely related to the metal nucleation behavior and surface structures of supports. For Pt ALD with trimethyl-(methylcyclopentadienyl)platinum (Me₃(MeCp)Pt), using H₂ as the second reagent shows smaller Pt size than the use of O₂, which was attributed to the activation of H₂ on Pt nanoparticles inducing the reduction of Pt and the depletion of surface hydroxyl groups [89]. Decreasing the size of noble metal particle is a direct method to increase the metal atom efficiency. Especially, single metal atom on support shows the maximum metal utilization. Supported single atom catalysts can also provide an ideal model for investigating the interfacial effects on catalyst activity,

which can shed light on designing more efficient automotive catalyst. As shown in figure 2(a), Lu *et al* utilized the surface defects on CeO₂ nanorods to anchor Pt single atoms during Pt ALD [53, 54]. Pt single atoms on the defects exhibited high stability due to the Pt–O–Ce bond interactions. Water in the feed gas could form surface hydroxyl groups on Pt₁/CeO₂ that accelerated CO oxidation following Mars-van Krevelen mechanism by yielding the carboxyl intermediate. Moreover, they reported the bottom-up precise synthesis of Pt dimers by selective deposition of additional Pt atoms on the Pt single atoms like Lego building blocks [90, 91]. The activity and stability of single atom catalysts are closely related to their local coordination environment [92–94]. For instance, the unique O_{lattice}[H] could be created in the vicinity of Pt²⁺ on CeO₂ after steam treatment at 750 °C, which not only greatly enhanced the low-temperature CO oxidation activity of CeO₂ supported Pt single atoms, but also exhibited outstanding hydrothermal stability [11, 95]. The migration and aggregation of single atoms are closely related to the free energy and density of adatoms on supports. By creating surface defective sites on supports or constructing atom ensemble catalysts, the single atom catalysts can exhibit superior activity and durability after aging at 900 °C [96, 97]. Recently, Liu *et al* reported a redox-coupled ALD method to prepare Pt single atoms and sub-nanoclusters on Cu doped CeO₂ supports (figure 2(b)) [55]. The coordination environment of interfacial Pt atom

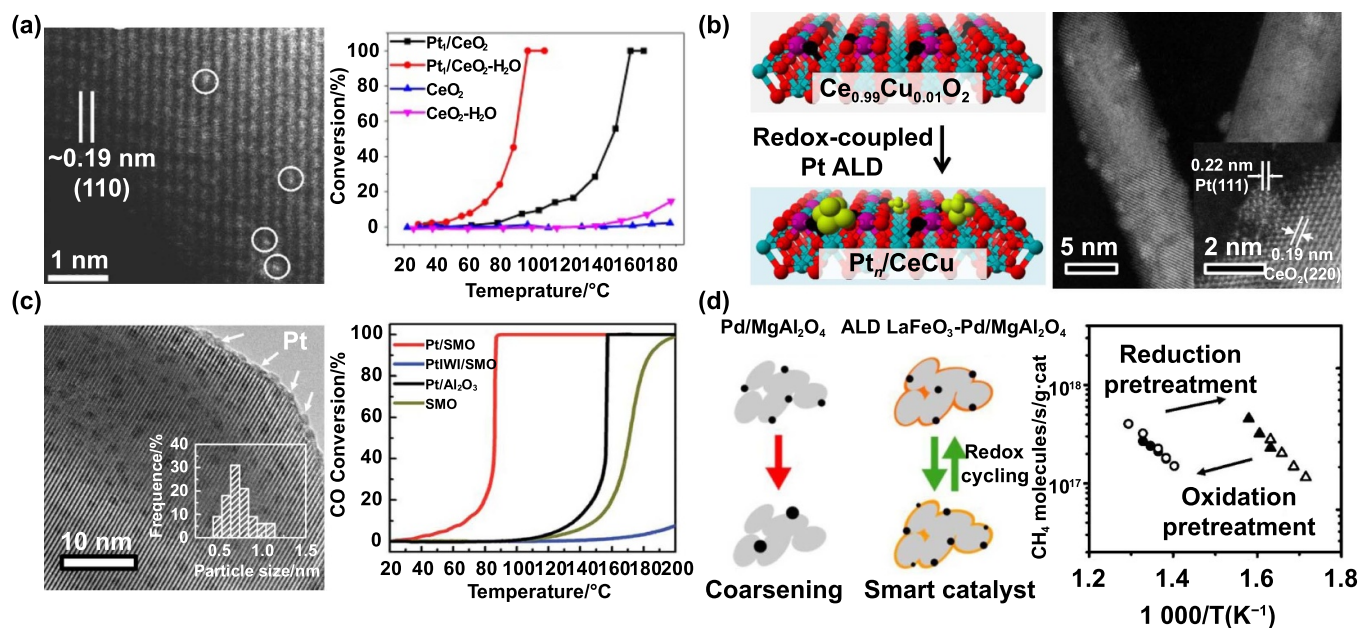


Figure 2. Metal oxide supported Pt catalysts prepared by ALD method. (a) Pt single atoms supported by CeO₂ nanorods. Reprinted with permission from [53]. Copyright (2017) American Chemical Society. (b) Cu doped CeO₂ nanorods supported Pt sub-nanoclusters. Reprinted with permission from Springer Nature Customer Service Centre GmbH: Springer Nature, Nature Communications [55], Copyright (2020). (c) SmMn₂O₅ mullite oxide supported Pt sub-nanoclusters. Reproduced from [61] with permission from the Royal Society of Chemistry. (d) Pd catalysts anchored by LaFeO₃ coatings prepared by ALD. Reprinted with permission from [69]. Copyright (2018) American Chemical Society.

could affect the activation of O₂ and adsorption strength of CO, while a moderate CO adsorption strength at the interface could facilitate the low-temperature CO oxidation performance. The sub-nanoclusters were formed by the aggregation of supported Pt single atoms under a reduced atmosphere, which showed remarkable CO oxidation performance with an onset temperature (T_{onset}) below room temperature and much higher turnover frequency (TOF) than atomically-dispersed Pt catalysts. Gao *et al* prepared size-controlled Pt nanoparticles on TiO₂ nano-arrays and CeO₂-based nanoflake arrays integrated on cordierite honeycombs, which exhibit good catalytic oxidation activities under the simulated exhaust condition of low-temperature diesel combustion [56, 57]. The 90% conversion temperature of CO and hydrocarbon over Pt/CeO₂ was about 180 °C. Li *et al* prepared highly dispersed Pt nanoparticles with the average size of 1.9 nm on SiO₂ supported by 5 cycles ALD of Pt, the TOF of which at 200 °C reached to 1.8 s⁻¹ [58].

Oxide supports are important for the dispersion of noble metal catalysts, the surface and bulk stability of which can also directly affect the durability of composite catalysts for frequently consuming and replenishing of surface oxygen species, as well as the high temperature working conditions. Compared with the simple transition metal oxides, such as CeO₂, FeO_x, Co₃O₄, the complex metal oxides with perovskite, mullite phase structures have been adopted for exhaust catalysis, due to their intrinsic activities and more stable atomic structures based on the backbone structure of connected metal-oxygen polyhedra [98–100]. Enterkin *et al* deposited size controlled Pt nanoparticles on perovskite SrTiO₃ nanocuboids by controlling the number of ALD cycles, which exhibited

a lower 50% conversion temperature (T_{50}) and higher stability for propane oxidation than a conventional Pt/Al₂O₃ catalyst [59]. By controlling the morphology of single crystal SrTiO₃ supports, Chen *et al* found that Pd ALD on SrTiO₃ nanocuboids with TiO₂-(001) exposed facet was more significant in size with the increase of the number of ALD cycles, while that on SrTiO₃ nanododecahedra with (110) exposed facet exhibited secondary nucleation and the density of Pd nanoparticles changed significantly [60]. Since the more edge and corner sites, smaller Pd nanoparticles (~2 nm) on SrTiO₃ supports exhibited higher TOF for CO oxidation than larger Pd nanoparticles with the size of ~3 nm. Different with perovskite oxides, Mn-based mullite oxide could expose the unique Mn-Mn dimer structure on the surface that was active for O₂ dissociation, which exhibited excellent NO oxidation activity [99, 100]. As shown in figure 2(c), Liu *et al* reported the SmMn₂O₅ mullite-type oxide supported Pt sub-nanoclusters catalyst by one cycle of Pt ALD [61]. The composite catalyst exhibited superior CO oxidation activity with the T_{50} of 86 °C and activation energy of 43.87 kJ mol⁻¹ due to the high activity of O₂ dissociation at Pt/SmMn₂O₅ bifunctional interface. The constructed Pt/SmMn₂O₅ bifunctional interface could provide spatially separated sites for CO and O₂, which served as an efficient poison-free CO oxidation site. Based on first-principles based microkinetics analysis, they designed the interfacial structure with Mn-Fe hetero-dimer that was predicted to further enhance the low temperature CO oxidation activity of Pt/SmMn₂O₅ catalyst [101]. In order to stabilize simple transition metal oxides, Onn and Gorte *et al* coated high-surface-area Al₂O₃ supports by CeO₂ or Co₃O₄ thin films to

produce composite catalyst supports for Pd [63–65]. The composite catalysts showed similar activity to CeO₂ or Co₃O₄ supported Pd catalysts for both CO and CH₄ oxidation, yet they can maintain their surface areas to much higher temperatures. Furthermore, Gorte *et al* synthesized high-surface-area LaFeO₃, CaTiO₃, LaCoO₃ perovskite-type coatings on MgAl₂O₄ supports by controlling the ALD cycles of simple oxides, Pt and Pd nanoparticles on which were found to be stabilized and switch between ‘active’ and ‘inactive’ states after high-temperature reduction or oxidation (figure 2(d)) [66–69]. These intelligent catalysts were closely related to the interaction between noble metal with the perovskite oxide films [102]. For instance, supported Pt nanoparticles could become part of the lattice of high-surface-area CaTiO₃ films under high temperature oxidizing condition due to the strong interaction between Pt with CaTiO₃, while support Pd catalysts on CaTiO₃ did not show this phenomenon [67]. Their recent work revealed the different interaction between Rh and three types of perovskite films, while the interaction strength affected the size of Rh after high temperature redox treatment, which followed the sequence of Rh/CaTiO₃/MgAl₂O₄ > Rh/SrTiO₃/MgAl₂O₄ > Rh/BaTiO₃/MgAl₂O₄ [103].

2.2. Encapsulated Pt group metal catalysts

Since the surface active sites are predominant in catalytic activity, the thermal stability of Pt group metal nanoparticle is an important factor leading to the decrease of active sites due to sintering at high temperature. Oxide overcoatings are created as physical barriers to minimize the agglomeration of Pt group metal nanoparticles at elevated working temperature, which need certain trade-off between stabilization and reactivity by controlling the process for the oxide shell growth. Owing to the precisely controlling of ALD on the film thickness, many encapsulation strategies have been developed to enhance the stability of Pt group metal nanoparticles and keep the exposure of surface active sites to reactants. The number of Al₂O₃ ALD cycles was controlled to prepare porous coatings on Pd nanoparticles by utilizing the nucleation stage of Al₂O₃ [104]. Lu *et al* reported a calcination post-treatment method to create ~2 nm micropores in ~8 nm Al₂O₃ coatings on Pd nanoparticles by removing the carbon residues caused by Al₂O₃ ALD process [105]. Based on this method, Duan *et al* coated Pd/SiO₂ catalyst by porous Al₂O₃ overlayers (figure 3(a)), large amounts of pentacoordinated Al³⁺ sites in which can stabilize the PdO_x phases resulting in enhanced activity and stability for methane combustion [70]. Cui *et al* also coated porous Al₂O₃ on Pd/Al₂O₃ by ALD, which effectively reduced the deactivation of Pd after sintering at 700 °C [71]. Furthermore, a porous Al₂O₃ coating layer was prepared by thermal decomposition of organic carbon chains in the alucone layer deposited by molecular layer deposition (MLD), which stabilized the supported Pt nanoparticles even at 800 °C [72]. Besides the thick and porous Al₂O₃ coating, some ultrathin films with the thickness smaller than 1 nm have been reported to stabilize Pt group metal nanoparticles. As shown in figure 3(b), Onn *et al* created a semicore-shell-like structure on PdO/Al₂O₃ catalyst by ~1 nm thick ZrO₂ coating after

calcination at 800 °C, which prevented the sintering of Pd and stabilized methane oxidation rates [73]. Onn *et al* modified Pd/CeO₂ by 0.4 nm ZrO₂ film, which maintained the activity for methane oxidation upon calcination to 800 °C [74]. The agglomeration of Pt particles on Al₂O₃ supports was mitigated by ~0.83 nm porous MnO_x coatings prepared by ALD [75].

In order to decrease the blocking of surface sites on Pt group metal nanoparticles by porous oxides, the selective ALD method has been developed to construct encapsulated nanostructures by control the nucleation and deposition of metal oxide on the desired areas or sites on the surface of catalysts. A low-temperature ABC-type ALD was reported to simultaneously deposit protected Pd nanoparticles and new support surface on TiO₂ supports. Pd nanoparticles were activated by removing the protective ligands after multiple ABC cycles [106]. Based on the unreactive template molecule or ligands, shape-selective sieving layers were prepared to stabilize single atom catalysts [107–109]. As shown in figure 3(c), Liu *et al* fabricated the Co₃O₄-nanotraps-anchored Pt nanoparticle structures on Al₂O₃ supports based on the blocked Co₃O₄ deposition on 1-octadecanethiol selectively covered Pt nanoparticles [76]. The surface Pt sites were re-exposed after removing the 1-octadecanethiol blocking agents via calcination in air. The formed Co₃O₄ nanotraps were regarded as physical barriers and exhibited strong interfacial interactions with Pt, which greatly improved the low temperature CO oxidation activity and thermal stability of Pt nanoparticles simultaneously. Without using the blocking agents, Chen *et al* have also found the inherent selective deposition behaviors of some metal oxides on different surface sites of Pt group metal nanoparticles that depend on the activity of precursors and deposition conditions. For instance, CeO_x was selectively deposited onto Pt (111) while leaving the Pt (100) surface intact, which was utilized to form nanofences around Pt nanoparticles (figure 3(d)). CeO₂ nanofence coated Pt nanoparticles exhibited sintering resistance at 700 °C in air and the excellent activity of the catalysts were retained after calcination [77]. Based on theoretical calculations, Wen *et al* found that the metal cyclopentadienyl precursors preferred to decomposition on the edge of Pt nanoparticles, indicating that edges were naturally selected to be covered during ALD of metal oxide using metal cyclopentadienyl precursors [110]. Nevertheless, AlO_x ALD with dimethylaluminum isopropoxide as Al precursor preferentially coated the Pt(111) facets [111]. The selective growth of FeO_x and NiO_x on the low coordination edges sites of Pt nanoparticles were achieved using the FeCp₂ and CoCp₂ precursors [78, 112]. Moreover, the NiO_x passivated Pt nanoparticles exhibited significantly enhanced sintering resistance after calcination at 750 °C in air due to the stabilization of volatile atoms at low coordinated sites on Pt nanoparticles. Besides selective ALD method, the confined structures of metal nanoparticles were reported to be constructed with the assistance of templates [113]. The micropores in a KL zeolite were utilized to confine Pt nanoclusters by controlling the size during Pt ALD, which prevented the agglomeration of Pt catalysts [114]. Qin *et al* developed a template-assisted ALD method to construct confined metal

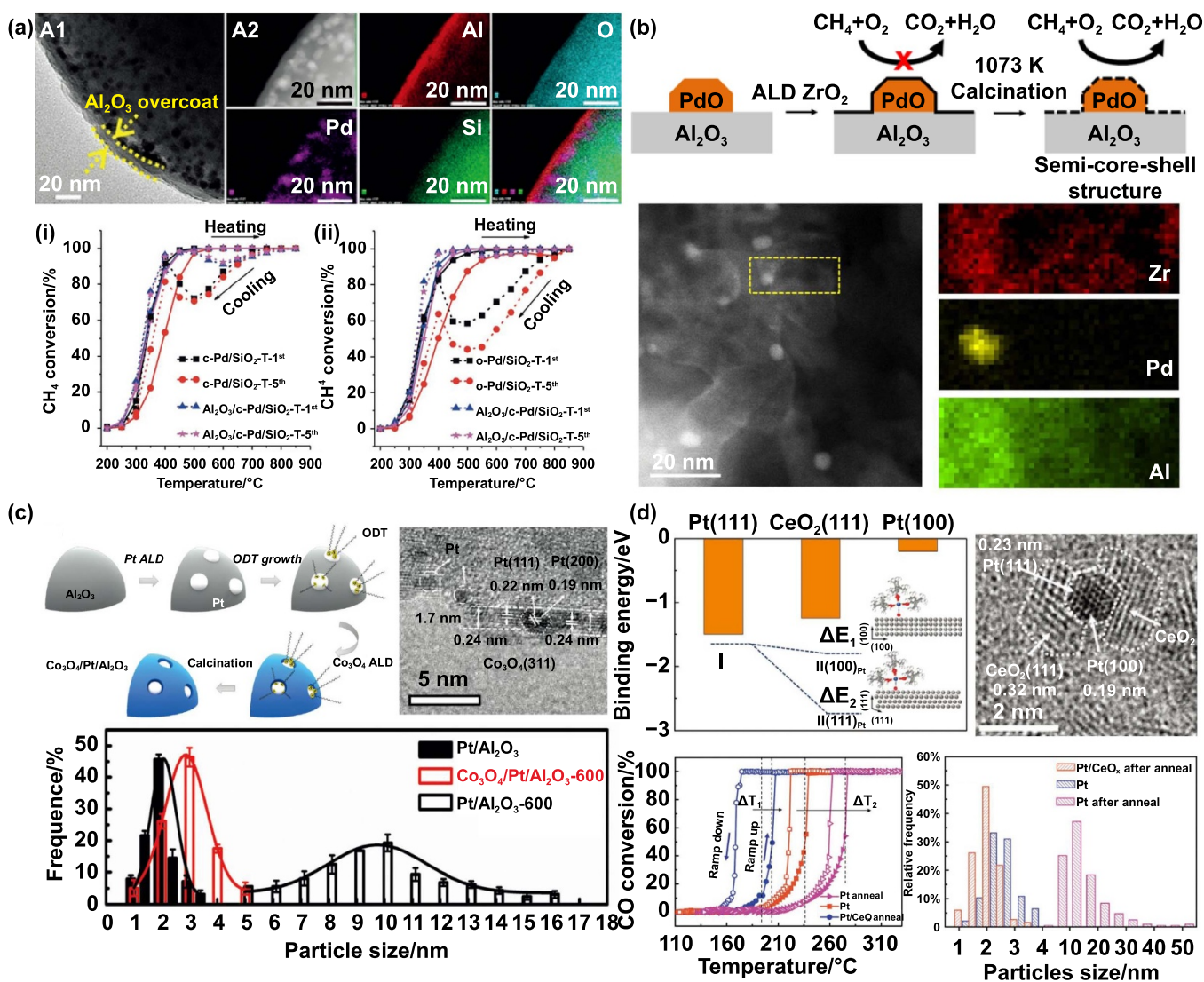


Figure 3. Pt group metal nanoparticles encapsulated by oxide coatings. (a) Pd nanoparticles embedded by porous Al_2O_3 overlayers. [70] John Wiley & Sons. © 2019 Wiley-VCH Verlag GmbH & Co. KGaA, Weinheim. (b) Semicore-shell-like structure composed by 1 nm ZrO_2 thin film and PdO nanoparticles. Reprinted with permission from [73]. Copyright (2015) American Chemical Society. (c) Co_3O_4 nanotrapers anchored Pt nanoparticles prepared by area-selective ALD. [76] John Wiley & Sons. © 2017 Wiley-VCH Verlag GmbH & Co. KGaA, Weinheim. (d) CeO_2 nanofence stabilized Pt nanoparticles by facet-selective ALD. [77] John Wiley & Sons. © 2017 WILEY-VCH Verlag GmbH & Co. KGaA, Weinheim.

nanoparticles. The metal oxide coated metal nanoparticles were firstly prepared on carbon nanocoils by ALD [115, 116]. As sacrificial templates, carbon nanocoils were subsequently removed by calcination treatment, resulting in the metal oxide nanotubes confined metal nanoparticles with enhanced stability.

2.3. Supported non-precious metal or oxide catalysts

Besides Pt group metal catalysts, many supported non-precious metal or oxide catalysts have also been prepared by ALD. For instance, Liang *et al* synthesized Fe single atoms on SiO_2 supports by optimizing the dose time of Fe precursor during ALD (figure 4(a)) [79]. SiO_2 supported Fe single atoms with high mass loading of 1.49 wt% exhibited much higher CO oxidation activity than other reported Fe-based

catalysts with the TOF of $\sim 0.011 \text{ s}^{-1}$ at 360 °C. Highly dispersed NiO_x nanoparticles with the average size of $\sim 1 \text{ nm}$ were deposited on mesoporous Al_2O_3 supports by ALD and subsequently annealing process, which exhibited high CO oxidation activity near room temperature and enhanced stability after calcination above 500 °C [80]. Jackson *et al* developed a CeO_2 and ZrO_2 coated Cu-exchanged ZSM-5 catalysts by ALD for NO_x removal from lean-diesel emissions using hydrocarbon catalyzed SCR [81]. Cu-exchanged ZSM-5 supports were modified by ZrO_2 deposited within the pore volume and $\text{ZrO}_2/\text{CeO}_2$ coated on the surface, which exhibited $\sim 40\%$ NO_x conversion at 350 °C. Amorphous TiO_2 domains supported highly dispersed VO_x species were prepared on mesoporous silica SBA-15 by ALD, which produced Si–O–V and Ti–O–V linkages [82]. The $\text{VO}_x/\text{TiO}_2/\text{SBA-15}$ catalyst exhibited 61.1% NO_x conversion with N_2 selectivity

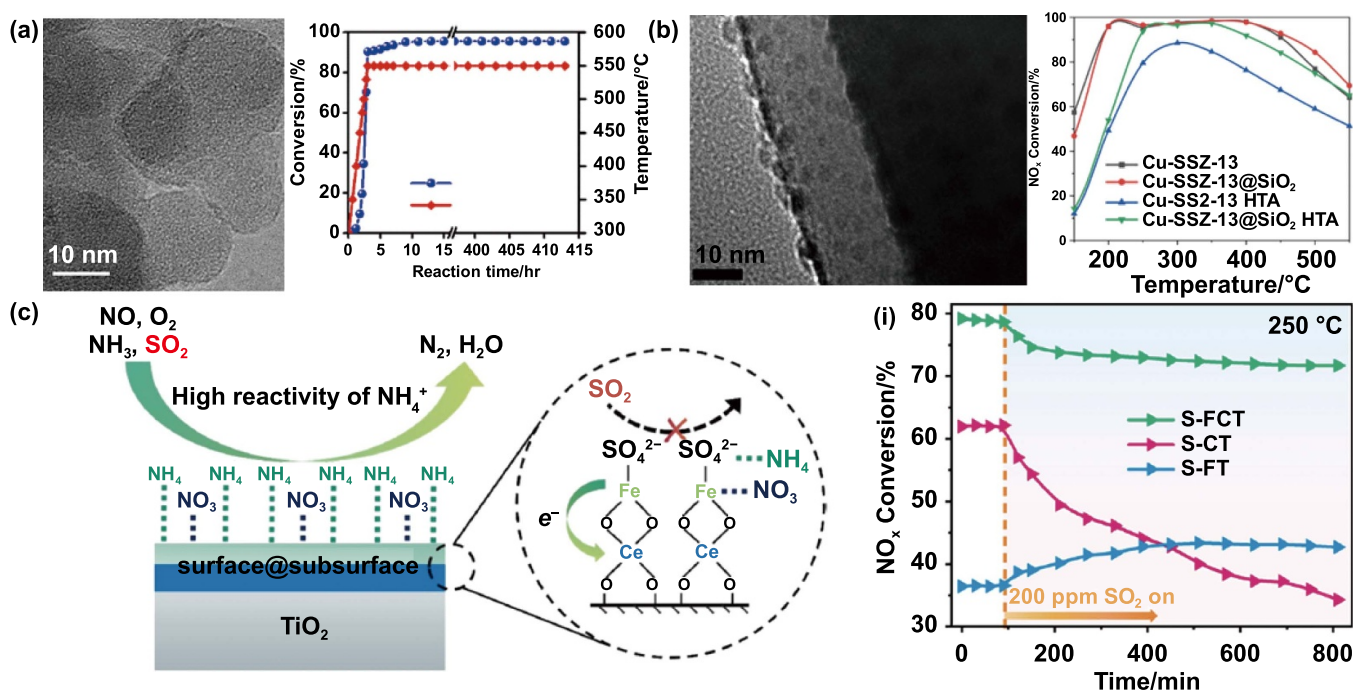


Figure 4. Supported metal or oxide catalysts prepared by ALD. (a) SiO₂ supported Fe single atoms for CO oxidation. Reprinted with permission from [79]. Copyright (2020) American Chemical Society. (b) SiO₂ coated Cu-SSZ-13 for NH₃ SCR of NO_x. Reprinted from [84], Copyright (2021), with permission from Elsevier. (c) Fe₂O₃ coated CeO₂/TiO₂ for NH₃ SCR of NO_x. Reprinted with permission from [85]. Copyright (2022) American Chemical Society.

of 98.1% at 250 °C due to the moderate acidity of highly dispersed VO_x on TiO₂/SBA-15. Sun *et al* selectively deposited TiO₂ on the oxygen-containing functional groups of graphene oxide to stabilize graphene oxide scrolled MnO₂ nanowires for SCR of NO_x [83]. TiO₂ modified graphene oxide greatly improved the steam and SO₂ resistance of MnO₂ catalyst for SCR of NO_x at low temperature by delaying the oxidizability of MnO₂. Furthermore, they coated SiO₂ on Cu-SSZ-13 to improve the high-temperature hydrothermal stability by suppressing the leaching of alumina from SSZ-13 molecular sieve (figure 4(b)) [84]. SiO₂ coated Cu-SSZ-13 showed the similar initial activity as Cu-SSZ-13 and remained considerable activity after ageing under moist air condition at 800 °C. As shown in figure 4(c), Qi *et al* coated Fe₂O₃ on CeO₂/TiO₂ catalysts to construct surface iron sulfate and subsurface CeO₂ structure by ALD and pre-sulfation method [85]. The electron transfer between surface Fe species and subsurface Ce species was tailored to improve the SO₂ tolerance of catalysts for NO_x reduction. Soot combustion is an important catalytic reaction for controlling the particulate soot emission from diesel vehicles. Ivanova *et al* deposited CeO₂ based thin films by ALD and found that the CeO₂ film deposited at 300 °C showed a better activity than CeO₂ deposited at low temperatures with the complete soot conversion temperature of 450 °C [86, 87].

3. Power lithium ion battery

At present, new energy vehicles powered by lithium ion battery are developing rapidly all over the world. Although the

power lithium ion batteries used in current electric vehicles can meet the basic requirements on energy density, there are still problems such as poor cycle stability and safety, which are closely related to the failure of battery materials. The performance of battery can be enhanced by atomic scale coatings on cathode, anode and separator by ALD that cannot only improve the electrochemical stability, but also ensure the transport of electrons and Li ions. The nanocoatings on the surface of cathode and anode materials can improve the structural stability of materials and suppress the side reactions between electrode and electrolyte during charge–discharge cycles. The enhanced mechanical performance and thermal stability of separator have also been reported after modified by ultrathin oxide films prepared by ALD.

3.1. Cathodes coated by ALD

Cathode can usually limit the specific energy of lithium ion battery that is determined by the specific capacity and nominal voltage of battery. At present, the commonly used cathode materials for power lithium ion battery are olivine-type LiFePO₄ and Ni-rich layer transition metal oxides (LiNi_xCo_yMn_{1-y-x}O₂, NCM, $x \geq 5$). Since the high working voltage and energy density, spinel type LiNi_{0.5}Mn_{1.5}O₄ is promising as the next generation cathode materials for electric vehicles. Table 2 has summarized the recently reported cathode materials modified by ALD and their electrochemical performances. Although LiFePO₄ exhibits excellent cyclic stability and intrinsic thermal stability, it suffers from poor rate performance and electrochemical stability at high

Table 2. Summary of cathode materials coated by ALD for lithium ion battery.

Cathode materials	ALD materials	Thickness/cycles	Electrochemical performance	References
LiFePO ₄	TiN	5 cycles	89% capacity retention rate after 1000 cycles at 2 C rate	[117]
LiFePO ₄	TiN	10 cycles	Improved rate performance and high temperature stability	[118]
LiFePO ₄	ZrO ₂	2 cycles	Reduced the undesirable side reactions between cathode and electrolytes	[119]
LiNi _{0.5} Co _{0.2} Mn _{0.3} O ₂	Al ₂ O ₃	1.65 nm	76.8% capacity retention rate after 30 cycles in the voltage range of 2–4.8 V	[120]
LiNi _{0.5} Co _{0.2} Mn _{0.3} O ₂	Al ₂ O ₃	30 cycles	Inhibited dissolution of transition metal in cathode materials during cycling	[121]
LiNi _{0.5} Co _{0.2} Mn _{0.3} O ₂	ZrO ₂	1 nm	73.4% capacity retention rate after 100 cycles at 0.5 C rate	[122]
LiNi _{0.5} Co _{0.2} Mn _{0.3} O ₂	ZrO ₂	5 cycles	88.1% capacity retention rate after 60 cycles at 5 C rate under 55 °C	[123]
LiNi _{0.5} Co _{0.2} Mn _{0.3} O ₂	ZnO	8 cycles	92.5% capacity retention rate after 60 cycles at 5 C rate under 55 °C	[124]
LiNi _{0.6} Co _{0.2} Mn _{0.2} O ₂	Al ₂ O ₃	4 and 10 cycles	Improved capacity retention by reducing the corrosion of electrode surface	[125]
LiNi _{0.6} Mn _{0.2} Co _{0.2} O ₂	Al ₂ O ₃	20 cycles	Improved cyclic stability at high cutoff voltages (4.3 V, 4.5 V and 4.7 V)	[126]
LiNi _{0.6} Co _{0.2} Mn _{0.2} O ₂	C-Al ₂ O ₃	20 cycles	93.5% capacity retention rate after 100 cycles at 1 C rate with the initial discharge capacity of 186.6 mA h g ⁻¹	[127]
LiNi _{0.6} Mn _{0.2} Co _{0.2} O ₂	Al ₂ O ₃	2 cycles	92.2% capacity retention rate after 300 cycles at 1 C rate	[128]
LiNi _{0.6} Co _{0.2} Mn _{0.2} O ₂	TiO ₂	5 nm	Initial discharge capacity of 187.7 mA h g ⁻¹ at 0.1 C and 85.9% capacity retention after 100 cycles at 1 C	[129]
LiNi _{0.8} Co _{0.1} Mn _{0.1} O ₂	Al ₂ O ₃	~10 nm	Improved the cycling performance by 40% in 2 Ah pouch cell	[130]
LiNi _{0.8} Co _{0.1} Mn _{0.1} O ₂	Al ₂ O ₃	~2 nm	Initial discharge capacity of 212.8 mA h g ⁻¹ and decay to 157.2 mA h g ⁻¹ after 100 cycles at 0.1 C	[131]
LiNi _{0.83} Mn _{0.05} Co _{0.12} O ₂	Al ₂ O ₃	~1 nm	Reduced the DC resistance and increased the cycling performance	[132]
LiNi _{0.8} Mn _{0.1} Co _{0.1} O ₂	Al ₂ O ₃	10 cycles	Reduced the alkalinity of cathodes and the extent of transition metal dissolution	[133]
LiNi _{0.8} Co _{0.1} Mn _{0.1} O ₂	TiN	20 cycles	70.9% capacity retention rate after 200 cycles at a current density of 100 mA g ⁻¹ in the voltage range of 2.8–4.5 V	[134]
LiNi _{0.8} Mn _{0.1} Co _{0.1} O ₂	LiAlF ₄	20 cycles	24% decay of capacity after 300 cycles with an electrochemical window of 2.75–4.50 V vs Li ⁺ /Li	[135]
LiNi _{0.8} Co _{0.1} Mn _{0.1} O ₂	Li _x Zr _y PO _z	~8 nm	80.5% capacity retention rate after 100 cycles at 1 C rate	[136]
LiMn _{1.5} Ni _{0.5} O ₄	Al ₂ O ₃	0.55 nm	Mitigated Mn dissolution from cathode	[137]
LiNi _{0.5} Mn _{1.5} O ₄	Al ₂ O ₃	<1 nm	98.0% capacity retention rate after 150 cycles at 0.5 C rate under 30 °C	[138]
LiNi _{0.5} Mn _{1.5} O ₄	Al ₂ O ₃	2 nm	93.7% capacity retention rate after 150 cycles at 0.5 C rate under 55 °C	[139]
LiNi _{0.5} Mn _{1.5} O ₄	TiO ₂	~2 nm	85.2% capacity retention rate after 350 cycles at 0.5 C under room temperature	[140]
LiNi _{0.5} Mn _{1.5} O ₄	TiO ₂	20 cycles	Improved capacity retention and coulombic efficiency in full cell	[141]
LiMn _{1.5} Ni _{0.5} O ₄	CeO ₂	~3 nm	97.4% capacity retention rate after 1000 cycles at 1 C rate under 55 °C	[142]
LiMn _{1.5} Ni _{0.5} O ₄	FeO _x	50 cycles	93.5% and 86.1% capacity retention under room temperature and 55 °C after 500 cycles at 1 C rate	[143]
LiNi _{0.5} Mn _{1.5} O ₄	LiAlO ₂	<1 nm	Stabilized electrodes as physical barriers in full cell	[144]
LiMn _{1.5} Ni _{0.5} O ₄	LiF	4 cycles	Improved protection against Mn dissolution	[145]
LiNi _{0.5} Mn _{1.5} O ₄	AlPO ₄	10 cycles	74.9% capacity retention rate after 350 cycles at 0.5 C rate	[146]
LiNi _{0.5} Mn _{1.5} O ₄	Li ₃ PO ₄ -TiO ₂	5 nm	81.2% capacity retention rate after 300 cycles at 0.5 C rate	[147]

temperatures due to its inherent low electronic- and ionic-conductivity. Liu *et al* deposited uniform and thin LiFePO₄ coatings on carbon nanotube by controlling the subcycles of Fe₂O₃, PO_x and Li₂O [148]. The LiFePO₄ and carbon nanotube composites showed excellent rate capability due to

the rapid Li⁺ insertion and extraction in LiFePO₄ coatings and improved electronic transfer between LiFePO₄ and carbon nanotubes. The rate capability of LiFePO₄ can also be enhanced by surface modification via ALD. As shown in figure 5(a), Gao *et al* coated 5 ALD cycles of TiN on LiFePO₄

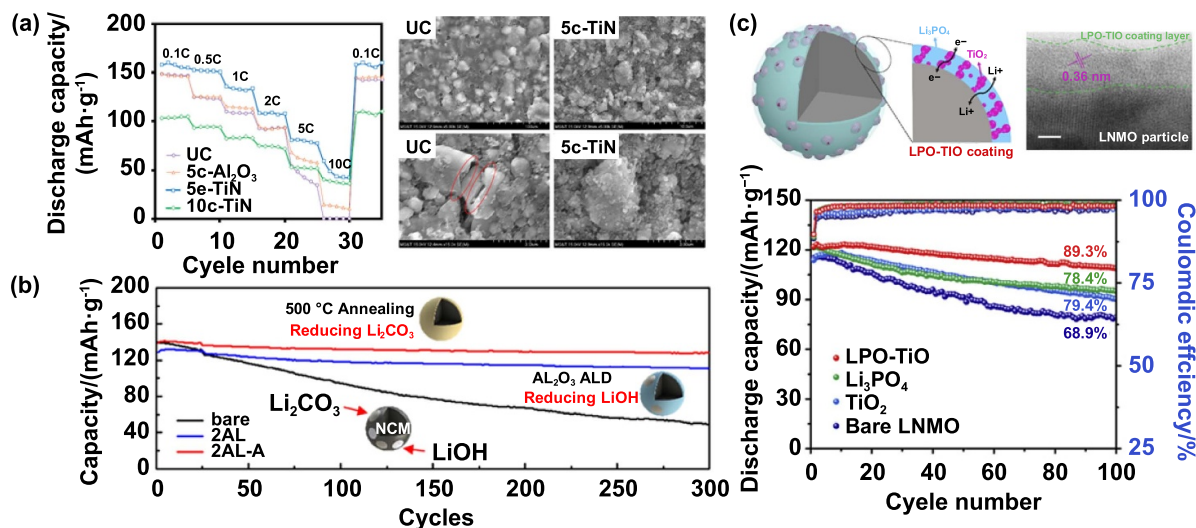


Figure 5. Cathode materials coated by ALD. (a) Rate performance and SEM images after 1000 charge–discharge cycles at 2 C rate of uncoated LiFePO₄ and 5 cycles TiN coated LiFePO₄. Reproduced from [117]. © The Author(s) 2018. Published by ECS. CC BY-NC-ND 4.0. (b) Cycling stability of bare and Al₂O₃ coated LiNi_{0.6}Co_{0.2}Mn_{0.2}O₂ at 1 C rate. Reproduced from [128]. CC BY 4.0. (c) Morphology of hybrid Li₃PO₄-TiO₂ coated LiNi_{0.5}Mn_{1.5}O₄ and the cyclic performance of bare and coated LiNi_{0.5}Mn_{1.5}O₄ at 0.5 C rate. Reprinted from [147], Copyright (2019), with permission from Elsevier.

that exhibited an improvement in both specific capacity and rate capability compared to those of uncoated LiFePO₄ [117]. From the scanning electron microscopy morphologies of uncoated and TiN coated LiFePO₄ after 1000 cycles at 2 C rate, the sample without ALD treatment showed a thick solid permeable interface layer and obvious cracks on the surface. Moreover, the TiN coating on LiFePO₄ can also improve the cyclic stability at a high temperature of 55 °C, which could suppress the dissolution of Fe at high temperature [118]. In the recent research, Jin *et al* carried out the deposition of ZrO₂ on LiFePO₄, which exhibited enhanced electrochemical performance in all solid state lithium battery due to the reduced undesirable side reactions between cathode and solid state electrolyte [119].

With the advantage of higher capacity than LiFePO₄, layered NCM materials are also widely used in electric vehicles. However, the poor intrinsic thermal stability of NCM and interface stability between NCM and electrolyte lead to the problems of cycling stability and safety, which become more severe with the increase of Ni content. Therefore, the surface modification by ALD is capable of improving the electrochemical performance of NCM materials. Al₂O₃ was the most common used coating on NCM materials, which improved the cycling performance of LiNi_{0.5}Co_{0.2}Mn_{0.3}O₂ by restraining the dissolution of transition metal in NCM [120, 121]. ZrO₂ and ZnO were reported to enhance the capacity retention and rate capability of LiNi_{0.5}Co_{0.2}Mn_{0.3}O₂ at high temperature or high voltage operation due to the suppressed undesirable side reaction [122–124]. For LiNi_{0.6}Co_{0.2}Mn_{0.2}O₂, conformal Al₂O₃ coatings were deposited on the cathode electrodes, which were served as physical barriers to prevent the surface corrosion of NCM particles and enhance the cycling performance at high charge voltages [125, 126]. The carbon and Al₂O₃ hybrid coating was prepared by the pyrolysis of organic

carbon chains in alucone coatings prepared by MLD, which improved the electrochemical kinetics of LiNi_{0.6}Co_{0.2}Mn_{0.2}O₂ by decreasing both charge and ion transfer resistance [127]. As shown in figure 5(b), Li *et al* reported that Al₂O₃ ALD coating coupled with post-annealing process in air reduced the residual lithium compounds on single-crystal LiNi_{0.6}Mn_{0.2}Co_{0.2}O₂ [128]. The post-annealing process induced the diffusion of Al atoms in cathode, which achieved 92.2% capacity retention after 300 cycles at 1 C rate. In addition to using Al₂O₃ as coating material, TiO₂ coating was also used to improve the cycling performance of LiNi_{0.6}Mn_{0.2}Co_{0.2}O₂ cathodes, which suppressed the interfacial parasitic reactions [129, 149]. When the content of Ni reaches to 80%, the capacity fading during cycling becomes more severe. Many researches have also reported that Al₂O₃ coatings on high Ni-content cathode materials can improve the capacity retention by suppressing phase transition and hydrofluoric acid-induced transition metal dissolution [130–133]. With the higher electrical conductivity than metal oxide, ultra-thin TiN layer was coated on LiNi_{0.8}Co_{0.1}Mn_{0.1}O₂ cathodes by ALD to accelerate the electron transport during the cycling [134]. Moreover, some lithium-containing coatings, such as LiAlF₄ and Li_xZr_yPO_z, were deposited to improve the rate performance and capacity retention due to their high lithium ion conductivity [135, 136].

Since the high working voltage of 4.7 V vs Li/Li⁺, absence of Co and good safety performance, spinel LiNi_{0.5}Mn_{1.5}O₄ has been regarded as a good alternative to NCM materials for next generation battery in electric vehicles [150]. However, such high working voltage induces many surface chemistry issues, such as Mn dissolution and side reactions between cathode and electrolyte, which lead to the capacity loss during cycling. Ultrathin Al₂O₃ coatings were prepared to improve the electrochemical stability at elevated temperature and suppress the self-discharge due to the mitigation of

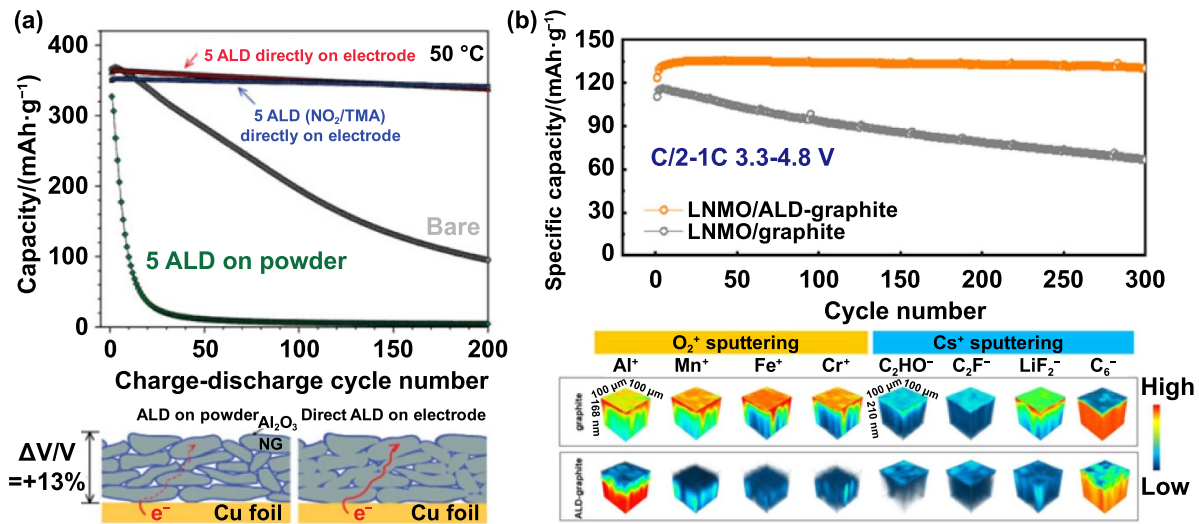


Figure 6. Anode materials coated by ALD. (a) Cycling stability of graphite electrodes with Al₂O₃ ALD on graphite powder or directly on electrode. [153] John Wiley & Sons. © 2010 WILEY-VCH Verlag GmbH & Co. KGaA, Weinheim. (b) Cycling performance of LiNi_{0.5}Mn_{1.5}O₄/graphite and LiNi_{0.5}Mn_{1.5}O₄/ALD-graphite full cells, as well as their electrode/electrolyte interfaces analysis after 300 cycles. Reprinted from [156], Copyright (2021), with permission from Elsevier.

Mn dissolution [137–139]. Xiao *et al* reported a method that included TiO₂ ALD and post-annealing treatment to optimize the performance of LiNi_{0.5}Mn_{1.5}O₄ [140]. The formed TiMn₂O₄-like spinel phase on the surface of LiNi_{0.5}Mn_{1.5}O₄ alleviated the decomposition of electrolyte. It was interesting that TiO₂ coated LiNi_{0.5-x}Mn_{1.5+x}O₄ revealed no improvement in the cycling stability in half-cells, while the improved stability was found in LiNi_{0.5-x}Mn_{1.5+x}O₄/graphite full-cells due to the retardation of transition metal by TiO₂ coatings [141]. Patel *et al* coated ~3 nm CeO₂ on LiMn_{1.5}Ni_{0.5}O₄ to mitigate Mn dissolution at elevated temperature, achieving ~97.4% capacity retention rate after 1000 cycles at 1 C rate under 55 °C [142]. Moreover, they found that FeO_x ALD followed by post-annealing treatment induced Fe doping in LiMn_{1.5}Ni_{0.5}O₄, which improved the Li⁺ transport and cyclic stability [143, 151]. In addition to coating these oxides, some lithium containing coatings (LiAlO₂, LiF) and AlPO₄ have been reported to suppress the dissolution of Mn and undesirable side reactions between LiNi_{0.5}Mn_{1.5}O₄ and electrolyte [144–146]. As shown in figure 5(c), a hybrid Li₃PO₄-TiO₂ coating was designed and prepared on LiNi_{0.5}Mn_{1.5}O₄ by ALD, in which Li₃PO₄ was considered as an ion conductive layer and TiO₂ was considered as an electron conductive layer. The hybrid coating not only provided sufficient ion and electronic conductivity, but also prevented the side reactions between cathode and electrolyte, which enhanced the cycling and rate performance of LiNi_{0.5}Mn_{1.5}O₄ [147].

3.2. Anodes coated by ALD

Although many high performance materials such as carbon-based, silicon-based and alloy materials are the promising anodes for power lithium ion battery, graphite is still the most widely used anode materials now, due to its low cost, high reversible capacity and moderate volume change [152]. In

order to enhance the cycling stability of lithium ion battery with graphite anode, ALD has also been performed to coat graphite by ultrathin oxide that can act as artificial solid electrolyte interface. For instance, Al₂O₃ was used to prevent electrolyte decomposition on the surface of natural graphite during initial charge–discharge [153]. As shown in figure 6(a), Lee *et al* compared the electrochemical performance of graphite electrodes with Al₂O₃ coated on graphite powder and Al₂O₃ directly coated on electrode. They found that Al₂O₃ coated on graphite powder exhibited poor capacity retention compared to bare materials due to the inhibited electron conduction between graphite powder and current collector, while the capacity retention was significantly enhanced after Al₂O₃ direct deposition on graphite electrode that enabled the electron transport. As a potential anode material, TiO₂ was also reported to modify the graphite electrode, which not only improved the cycling stability at elevated temperature, but also increased the initial discharge capacity [154]. Besides acting as artificial solid electrolyte interface, metal oxide coatings on graphite can also inhibit the formation of soluble byproducts, such as radicals, RO₂Li, which can diffuse to positive electrode and participate in the side reactions [155]. As shown in figure 6(b), the ultra-thin Al₂O₃ coating on graphite (ALD-graphite) drastically improved the cycling stability of LiNi_{0.5}Mn_{1.5}O₄/graphite full cell due to the isolation of graphite from electrolyte and inhibition of undesired side reactions [156]. Furthermore, the time-of-flight-secondary ions mass spectrometry analysis was performed to study the electrode/electrolyte interfaces after charge–discharge cycling, the results of which revealed that Al₂O₃ coating on graphite anode reduced the formation of HF by decomposing LiPF₆ and inhibited the attack of HF on both graphite anode and LiNi_{0.5}Mn_{1.5}O₄ cathode. In addition to graphite, Si-based materials have also attracted much attention to lithium ion battery due to the high theoretical capacity. However, the large

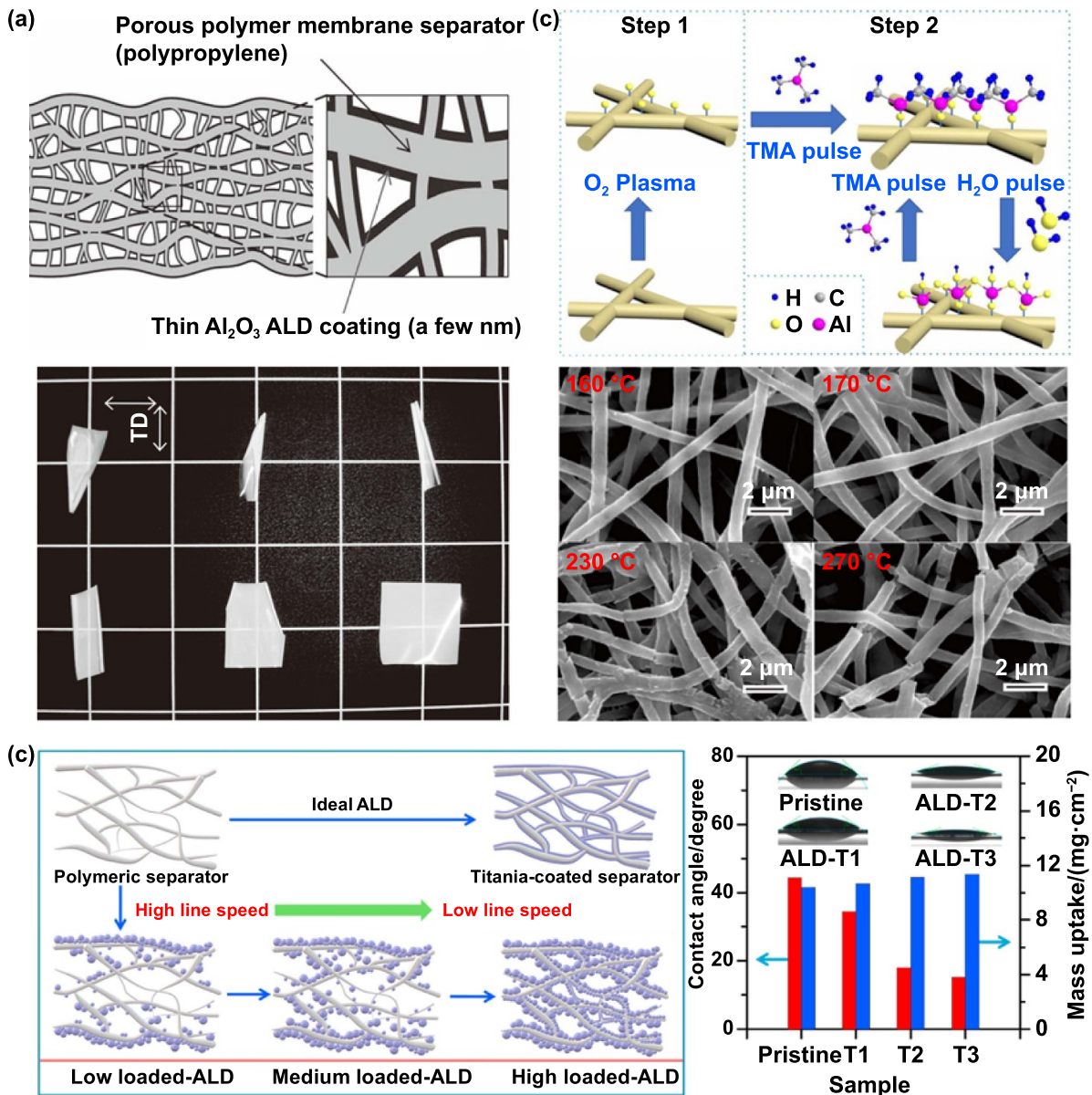


Figure 7. Separators modified by ALD. (a) Schematic diagram and thermal shrinkage of ALD-coated porous polymer membrane separator. [50] John Wiley & Sons. © 2012 WILEY-VCH Verlag GmbH & Co. KGaA, Weinheim. (b) Schematic diagram of ALD modification on nonwoven separator and SEM images after heat treatment under different temperatures. Reprinted from [163], Copyright (2018), with permission from Elsevier. (c) Schematic diagram of separator modified by roll-to-roll ALD system and the contact angle analysis of separators with different ALD loadings. Reprinted from [165], Copyright (2021), with permission from Elsevier.

volume change makes Si-based materials suffer from rapid capacity fading during charge–discharge cycling. Si/C composite with buffer effect on volume change and enhanced electron conductivity is considered as the most promising anode materials to make their way into the large-scale market. Conformal Al₂O₃ coating was deposited on Si/C composite nanofiber anodes, which increased the capacity retention after 100 charge–discharge cycles by improving the mechanical integrity of electrode structure and preventing the side reactions between anode materials and electrolyte [157]. Furthermore, Al₂O₃ was also directly deposited on Si-graphene composite electrode to improve the cycling performance by suppressing the side reactions [158].

3.3. Separator modified by ALD

Although the separator does not directly participate in the electrochemical processes, it is responsible for the improvement of lithium ion battery performance and safety. Since ALD is based on the alternative reactions between precursors and substrate including pore walls, many membranes are reported to be modified by ALD to adjust the pore sizes or to establish new separation layers to enhance selectivity and permeability [159]. At present, polyolefin-type separators, such as polyethylene and polypropylene membranes are commonly used due to their good mechanical strength and chemical stability at mild temperature, which can meet the basic needs of

separator for lithium ion battery. However, these polyolefin-type separators are prone to shrinkage and deformation at high temperature due to their low melting points, resulting in the internal short circuit and speeding up thermal runaway of lithium ion battery [160, 161]. Some metal oxides deposited by ALD have been applied to modify the surface of separator to enhance the thermal stability, which can keep the thickness of separator. As shown in figure 7(a), Al_2O_3 nano coatings were deposited on the surface of polypropylene microframework, which resulted in the unchanged thickness compared to the conventional ceramic coated separator. Meanwhile, the Al_2O_3 coated polypropylene separator exhibited improved stability at 160 °C and wettability in polar electrolyte, as well as unchanged electrochemical performance [50]. In order to decrease the thickness of ALD coating, Wang *et al* introduced plasma pretreatment to increase the active groups on polypropylene separator that resulted in the conformally coating of TiO_2 by 20 ALD cycles. The thin TiO_2 coating not only suppressed the thermal shrinkage and improved the wettability of polypropylene separator, but also increased the specific discharge capacities at variable rates due to an increase of pore size in polypropylene separator [162]. Besides polyolefin-type separators, the polyvinylidene fluoride-hexafluoropropylene nonwoven separator has also been modified by ALD coatings. As shown in figure 7(b), Al_2O_3 ALD was performed on nanofiber separator after O_2 plasma treatment. Al_2O_3 coated separator exhibited drastically improved safety performance with the stable morphology after heat treatment at 270 °C, while the bare separator turned into ribbon type at 160 °C [163, 164]. In order to increase ALD coating rate on separator, a roll-to-roll ALD system was designed including ALD shower arrays, oxygen radio-frequency plasma reactor, gas delivering sub-systems and vacuum pumping units [165]. As shown in figure 7(c), the moving speed of separator in roll-to-roll ALD system was investigated, which could affect the uniformity and mass loading of ALD coatings, as well as the contact angle of electrolyte on separator.

4. Hydrogen fuel cell

Although hydrogen fuel cell a promising alternative due to its high theoretical efficiency and power density, as well as environmental friendliness, the high cost and poor durability are the most obstacles for its scale commercial application in vehicle. As the core component of hydrogen fuel cell, MEA is widely studied to evaluate the performance of functional components, such as catalyst layer, gas diffusion layer and proton exchange membrane. Since the sluggish kinetics of oxygen reduction reaction (ORR) at the cathode of hydrogen fuel cell, large amounts of Pt catalyst are required in the catalyst layer, resulting in the high cost of hydrogen fuel cell. Highly dispersed Pt catalysts with controlled size have been prepared by ALD method, which can not only increase the utilization of Pt, but also decrease the O_2 transfer resistance in the catalyst layer. Furthermore, ALD has been utilized to modify Pt catalysts and conductive supports to enhance the intrinsic catalytic activity and stability. In the MEA

level, the surface modification of catalyst layer, gas diffusion layer and proton exchange membrane has been performed to increase the mass transport and durability of hydrogen fuel cell.

4.1. Preparation of supported Pt catalysts

Different from exhaust gas catalysts, Pt catalysts for hydrogen fuel cells are usually supported by carbon based supports that can satisfy the requirements of high electron conductivity and corrosion resistance under fuel cell condition as listed in table 3. Although well dispersed Pt catalysts with controllable size are achieved by ALD on oxide supports, carbon based supports with high specific surface area or low surface nucleation sites need some pre-treatments and special ALD processes [184, 185]. By using long pulse and purge times to maximize penetration of the ALD precursors into and removal of byproducts out of supports, King *et al* deposited Pt nanoparticles with narrow size distribution on carbon aerogels with appreciable surface area of $\sim 480 \text{ m}^2 \text{ g}^{-1}$ [186]. Since bare nucleation sites on carbon nanotubes, Perng *et al* deposited uniform and well-distributed Pt nanoparticles on acid-treated carbon nanotubes, which exhibited a higher specific power density in MEA than commercial Pt/C catalysts [166, 167]. Hsieh *et al* studied the two self-limiting reactions during Pt ALD using methylcyclopentadienyl-(trimethyl) platinum (MeCpPtMe_3) and oxygen and found a linear increase of Pt mass loading on carbon nanotubes with the ALD cycles [168, 169]. By comparing the growth behaviors of Pt using O_2 and H_2 as the second precursor, Lubers *et al* found that oxygen induced the combustion of carbon supports and the aggregation of Pt after Pt precursor attached on the surface of carbon supports, while hydrogen removed the ligands of Pt precursor by hydrogenation reactions that did not recreate surface functionalization, leading to the smaller size of Pt nanoparticles [187].

In order to uniformly deposit Pt nanoparticles on carbon black supports, Lee *et al* filtered the carbon supports and controlled their size within the range of 60–100 μm that ensured the homogenous fluidization during ALD process (figure 8(a)) [170]. The size of Pt nanoparticles were controlled by changing the number of ALD cycles, while the highly dispersed and dense Pt nanoparticles with the size of $\sim 1 \text{ nm}$ were prepared by 5 cycles of Pt ALD. The further increased ALD cycles could result in size increase and agglomerate of Pt due to preferential adsorption and reaction of Pt precursor occurring on previously deposited Pt nanoparticles. Nonetheless, the number of ALD cycle was optimized to about 15–20 for the best fuel cell performance, which ensured the Pt diameter of 2–3 nm that could exhibit the highest mass activity and satisfy the requirement for mass transfer [170, 171]. The optimized Pt size was also reported as $\sim 2 \text{ nm}$ on carbon nanotubes for ORR [172]. In order to increase the utilization of Pt, Xu *et al* reported a passivation-gas incorporated ALD method using CO molecules as the growth inhibitors to suppress the thickness increase of Pt nanoparticles [173]. CO molecules promoted two-dimensional growth of Pt nanoparticles with a more than 40% improvement in Pt

Table 3. Summary of supported Pt catalysts prepared by ALD for hydrogen fuel cell.

Fuel cell catalyst	ALD material	Size of Pt based catalyst (nm)	Role of ALD	Catalytic performance	References
Pt/CNT	Pt	/	Conformal deposition of Pt nanoparticles	Maximum power density for MEA: 0.17 W cm ⁻²	[166]
Pt/CNT	Pt	6.4 nm	Controlling size and number of Pt nanoparticles	Specific power density at 0.6 V: 2.692 W mg _{Pt} ⁻¹	[167]
Pt/CNT	Pt	3–5 nm	Well dispersed Pt nanoparticles	Maximum power density for MEA: 2.95 kW g _{Pt} ⁻¹	[168]
Pt/CNT#GO hybrids	Pt	3.95 nm (100 cycles)	Well dispersed Pt nanoparticles	Maximum power density for MEA: 2.32 kW g _{Pt} ⁻¹	[169]
Pt/C	Pt	3.00 nm (20 cycles)	Narrow size distribution and controllable size of Pt	Current density at 0.6 V for MEA: 1.58 A cm ⁻²	[170]
Pt/functionalized carbon	Pt	1.5–2.5 nm	Highly dense and uniform Pt nanoparticles	Current density at 0.6 V for MEA: 1.54 A cm ⁻² ; decrease to 1.26 A cm ⁻² after 30k cycling test	[171]
Pt/CNT	Pt	1.9 nm (20 cycles)	Well-controlled Pt particle sizes and distributions; desirable Pt ⁰ 4f binding energy; Cl-free Pt surfaces	1.4 times higher mass activity than the commercial 20% Pt/C catalyst for ORR	[172]
Pt/C	Pt	3.1 nm	Controlling the morphology of Pt	Mass activity at 0.9 V: 1.16 A mg _{Pt} ⁻¹ ; 10% loss of electrochemically active area after 10 000 cycles of the ADT	[173]
Pd ₃ Au@Pt/C	Pt	5.5 nm	Preparation of thin Pt shell	Mass activity at 0.9 V: 558 mA mg _{Pt} ⁻¹	[174]
Pt ₁ /Pd/NCNT	Pt	Single atoms	Preparation of Pt single atom catalyst	Electrochemical surface area: 32.4 m ² g _{Pt} ⁻¹ ; specific activity at 0.9 V: 0.12 mA cm _{Pt} ⁻² ; mass activity at 0.9 V: 0.91 A mg _{Pt} ⁻¹	[175]
Pt ₁ /ZIF-NC	Pt	Single atoms	Size-controlled Pt catalysts	Electrochemical surface area: 229 m ² g _{Pt} ⁻¹ ; specific activity at 0.9 V: 0.51 mA cm _{Pt} ⁻² ; mass activity at 0.9 V: 1.17 A mg _{Pt} ⁻¹	[176]
Pt/ZrC	Pt	2–4 nm	Improving the strong metal–support interactions at the atomic level	Mass activity at 0.9 V: 0.122 A mg _{Pt} ⁻¹	[177]
Pt/Mo ₂ C	Pt	/	Providing atomic level size control of Pt nanoparticles	Peak power density for MEA: 414 mW cm ⁻²	[178]
Pt/TiN	Pt	10.15 nm	Controlling the uniformity and size of Pt	Specific power density of MEA at 0.6 V: 1.061 kW g _{Pt} ⁻¹ ; maximum power density for MEA: 0.071 W cm ⁻²	[179]
Pt/TiN	Pt	~2.3 nm	Fine control of Pt size	Half-wave potential is 20 mV higher than that of commercial Pt/C	[180]
Pt/Nb-TiO ₂	Pt	/	Preparation of uniform Pt nanoparticles	Specific activity at 0.9 V: 0.28 mA cm _{Pt} ⁻²	[181]
Pt/Sb-doped SnO ₂	Pt	~2.6 nm	Precise control of the particle size of Pt	Electrochemical surface area: 74 m ² g _{Pt} ⁻¹ ; mass activity at 0.9 V: 102 mA mg _{Pt} ⁻¹	[182]
Pt/CeO ₂ /CNT	Pt	~2.5 nm	Constructing effective triple junction interface	Electrochemical surface area: 74.13 m ² g _{Pt} ⁻¹ ; half-wave potential: 0.865 V	[183]

surface-to-volume ratio that resulted in the high mass activity for ORR. Liu *et al* prepared Pd₃Au@Pt core@shell structure by selective ALD to increase Pt usage efficiency. Owing to the block of surfactant molecules on carbon supports and the catalytic decomposition of Pt precursors on Pd₃Au, a Pt shell was selectively deposited on Pd₃Au nanoparticles instead of on

carbon, which exhibited a significantly improved mass activity for ORR compared with commercial Pt/C [174]. As shown in figures 8(b) and (c), Sun *et al* deposited Pt single atoms on Pd nanoparticles or metal-organic framework (MOF)-derived N-doped carbon to maximum the utilization of Pt, which delivered 4 or 6.5 times higher mass activity than that of Pt

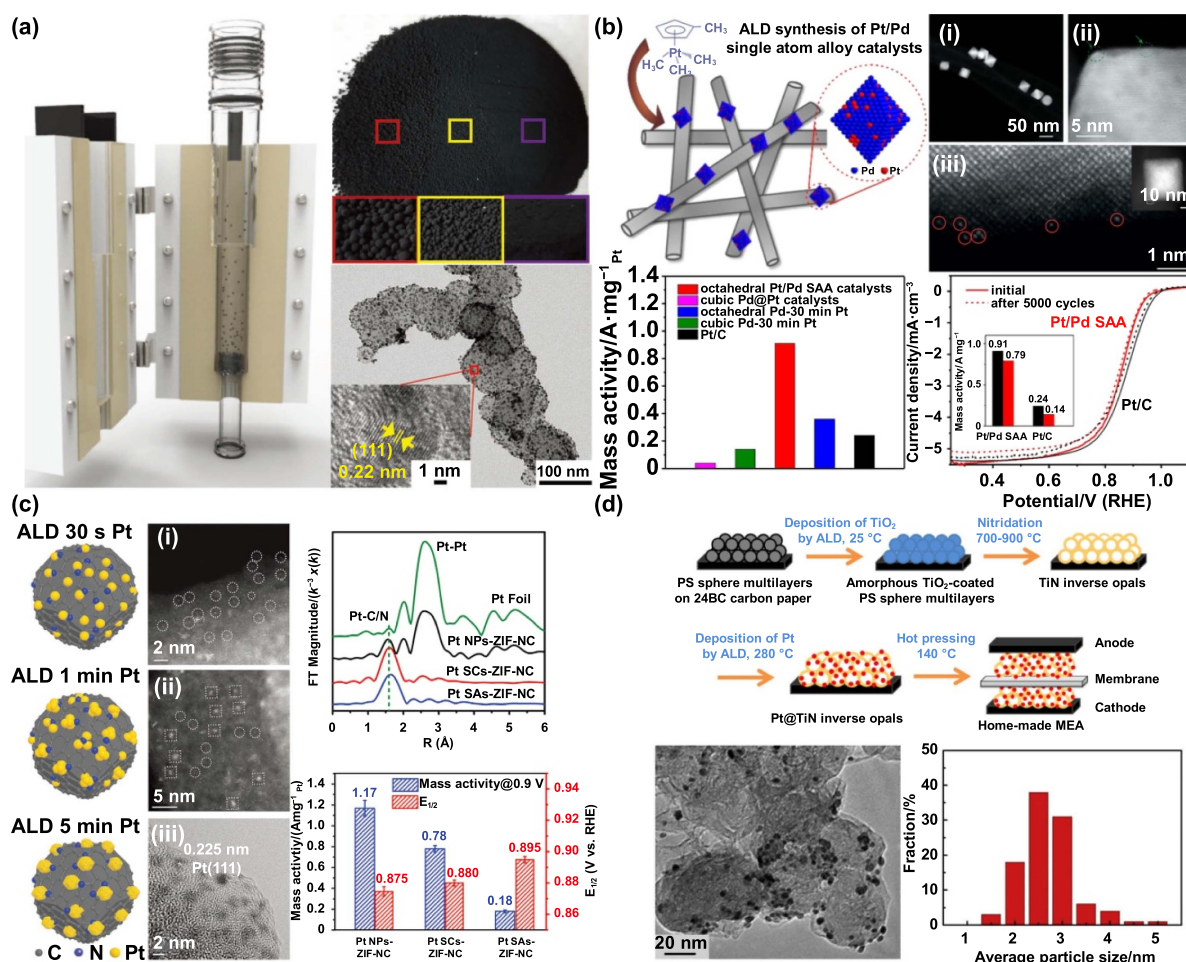


Figure 8. Pt catalysts on carbon based supports or carbides prepared by ALD. (a) Carbon supported Pt nanoparticles prepared by fluidized bed ALD. [170] John Wiley & Sons. © 2019 WILEY-VCH Verlag GmbH & Co. KGaA, Weinheim. (b) Pt single atoms on Pd nanoparticles for ORR. Reprinted with permission from [175]. Copyright (2019) American Chemical Society. (c) Pt single atoms, clusters and nanoparticles on MOF-derived N-doped carbon. [176] John Wiley & Sons. © 2020 Wiley-VCH GmbH. (d) TiN supported Pt nanoparticles with strong metal-support interactions. Reprinted from [179]. Copyright (2017), with permission from Elsevier.

nanoparticles for ORR [175, 176]. The Pt single atoms were anchored by the pyridinic N sites on the MOF-derived N-doped carbon supports. Due to the low-coordination environment and interaction between Pt atoms and nitrogen-doping sites, the electronic structures of Pt single atoms were versatile with different adsorption intermediates, while the multichannel reaction mechanism of oxygen reduction reaction on Pt single atoms exhibited lowered free energy change for the rate-determining step.

Although carbon black is widely used as support for Pt catalysts, it usually suffers from low resistance to electrochemical corrosion under the working condition of hydrogen fuel cell, leading to the detachment and aggregation of Pt catalysts [188, 189]. Lots of carbon-alternative materials, such as carbides, nitrides and metal oxides, have been studied, which own sufficient electrical conductivity, high resistance to electrochemical corrosion, as well as strong interaction between the support and Pt. Similar as carbon black, Pt ALD on carbide is also following an island growth mechanism [190]. Cheng *et al* deposited uniform Pt nanoparticles with

the average size of 3.2 nm on corrosion-resistant ZrC supports by controlling the number of Pt ALD cycles [177]. Since the strong interactions between Pt nanoparticles and ZrC supports, Pt nanoparticles deposited by ALD showed high total unoccupied density of states of Pt 5d character, which exhibited higher ORR activity and durability than Pt nanoparticles prepared by a conventional chemical reduction method. The performance of Pt/Mo₂C prepared by ALD was evaluated in a MEA, which showed higher power density than commercial Pt/C after accelerated degradation test [178, 191]. Besides carbides, TiN was also used as a support of Pt nanoparticles prepared by ALD (figure 8(d)), which exhibited enhanced ORR performance due to the good conductivity and corrosion resistance of TiN, as well as the strong interactions between Pt and TiN support [179, 180]. Nb doped TiO₂ and Sb doped SnO₂ were also reported to promote the ORR catalytic activity and stability of uniform Pt nanoparticles prepared by ALD [181, 182]. Especially, a triple junction interface composed by carbon support, oxide and Pt nanoparticle was constructed by ALD, which could overcome the problems of oxide,

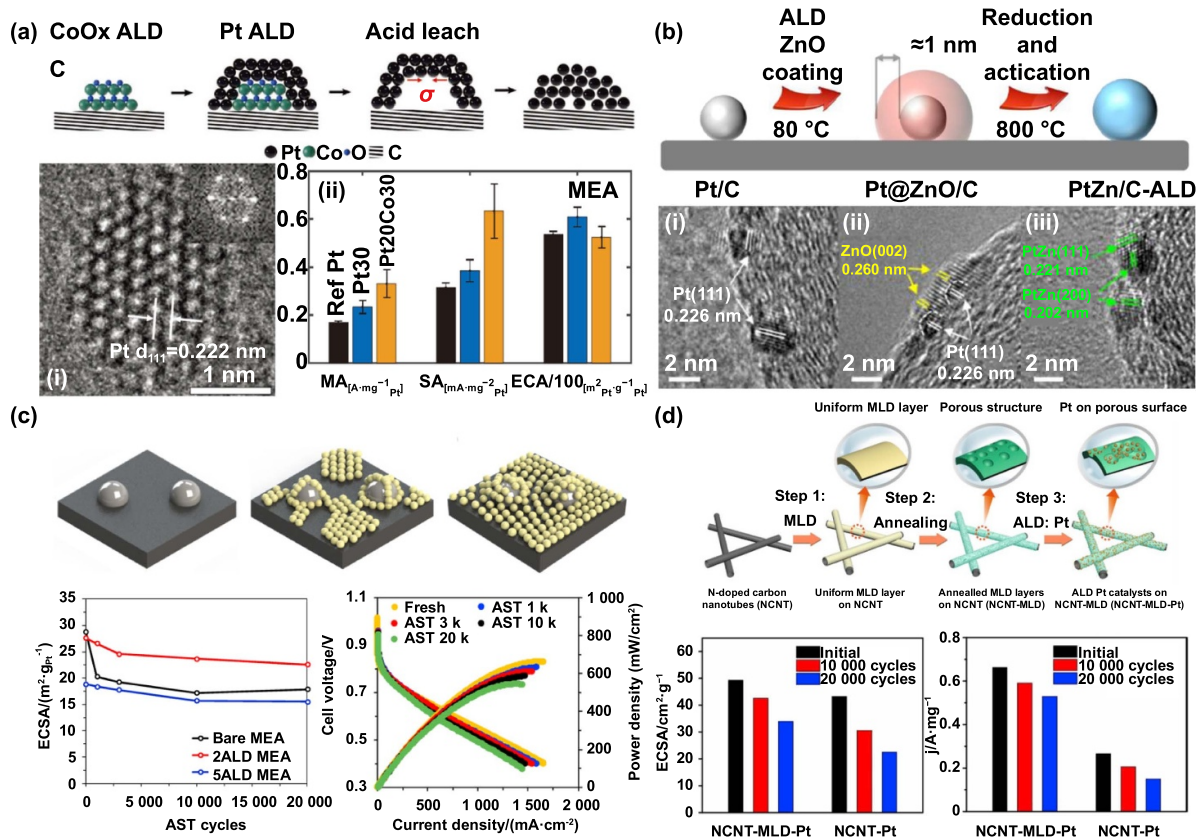


Figure 9. Modifications of Pt and carbon supports by ALD. (a) Lattice-strained Pt catalysts achieved by leaching CoO_x core from a Pt shell prepared by ALD. [194] John Wiley & Sons. © 2021 The Authors. Advanced Materials published by Wiley-VCH GmbH. (b) Uniform sub-3 nm PtZn intermetallic nanocrystals constructed by selectively ultra-thin ZnO coating on Pt nanoparticles. Reprinted from [200], Copyright (2023), with permission from Elsevier. (c) Coating of supported Pt nanoparticles by porous ZrO₂ layer at the atomic scale. Reprinted from [201], Copyright (2021), with permission from Elsevier. (d) MLD-derived coatings on nitrogen-doped carbon nanotubes with enriched pores to anchor Pt nanoparticles. Reprinted from [202], Copyright (2019), with permission from Elsevier.

such as limited conductivity and small specific surface area [183, 192, 193].

4.2. Modifications of Pt and supports by ALD

Compared with pure Pt nanoparticles, Pt catalysts modified by strain engineering or alloying have been designed and achieved by ALD, which exhibit enhanced intrinsic catalytic activity and stability for hydrogen fuel cell. As shown in figure 9(a), Xu *et al* sequentially deposited CoO_x and Pt on supports, and prepared the lattice strained Pt catalysts by dissolving the CoO_x core with acid [194]. The Pt lattice compression was confirmed by the Pt-Pt distance analysis from the results of x-ray absorption spectroscopy and transmission electron microscopy, which resulted in the mass activity at 0.9 V for MEA close to 0.8 A mg_{Pt}⁻¹. By varying the number and order of Pt and Co precursor cycles, the PtCo alloy nanoparticles with narrow particle size distribution and high metal dispersion were prepared by ALD, which exhibited positive onset potential and larger limiting current than Pt/C [195]. Pt₇₅Ni₂₅, Pt₇₈Ni₂₂, Pt₈₁Ni₁₉ and Pt₈₅Ni₁₅ alloy with the average size of ~2 nm were synthesized by tuning the super-cycle ratio, in which Pt₇₈Ni₂₂ was converted into the Pt skin-Pt₃Ni alloy structure after heat treatment resulting in

a high MEA performance with the mass activity at 0.9 V of 0.375 A mg_{Pt}⁻¹ [196]. Based on the precisely control over the deposition of single atoms, the prepared Co single atoms modified Pt nanoparticles exhibited significantly improved activity and stability for ORR compared to commercial Pt/C [197]. Besides the sequentially deposition of Pt and metal, ALD of Pt and metal oxide in combination with a subsequent reduction step was also performed to prepare Pt alloys. For instance, Pt₃Ti and PtZn alloy nanoparticles were synthesized by reducing Pt and TiO₂ or ZnO at different temperature, the average sizes of which were ~10 nm and ~3 nm, respectively [198, 199]. As shown in figure 9(b), Chen *et al* recently reported a strategy to construct uniform sub-3 nm Pt-based intermetallic nanocrystals based on selectively ultra-thin metal oxide coating on Pt nanoparticles via ALD [200]. Area-selective and thickness controllable ZnO coatings were performed to prepare uniform PtZn intermetallic nanocrystals with the size of 2.50 ± 0.65 nm, which could provide Zn atoms for alloying and prevent the sintering of Pt nanoparticles during ordering reduction. The outstanding MEA performance with peak power density of 1.56 W cm⁻² and 10.42% loss in mass activity after 30 000 voltage cycles was achieved, which was attributed to the decreased binding energy of Pt-oxygen intermediates for weakly polarized surface Pt atoms

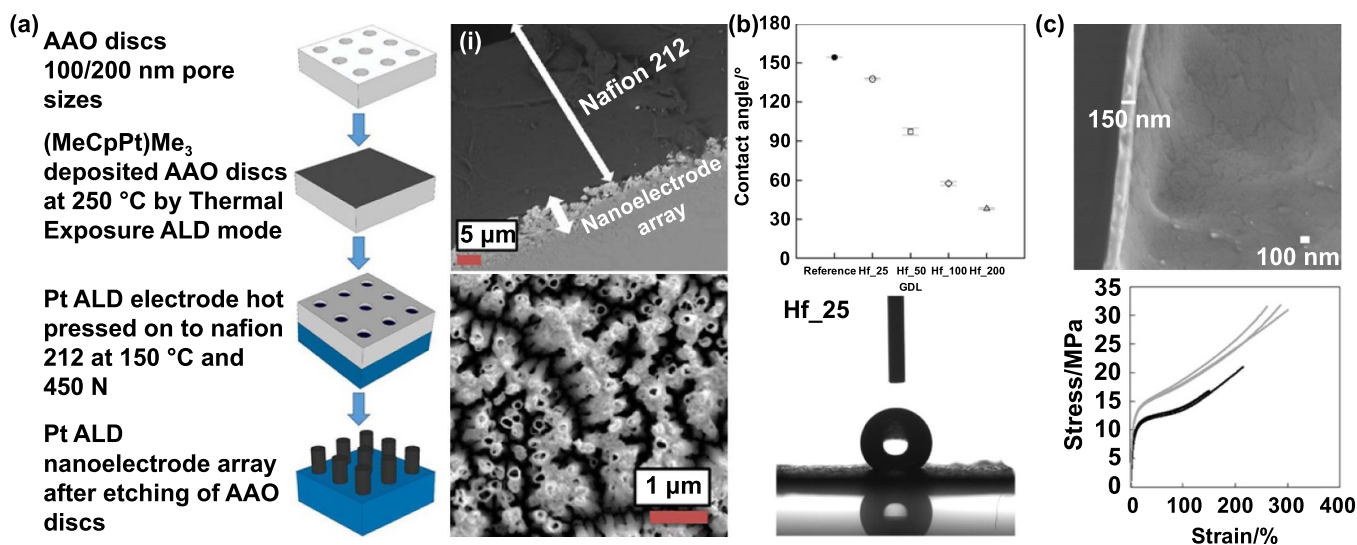


Figure 10. Modifications of the functional components in MEA by ALD. (a) Pt nanoelectrode array prepared by ALD assisted by anodized aluminium oxide template. Reproduced from [215]. © The Author(s). Published by IOP Publishing Ltd. CC BY 4.0. (b) Gas diffusion layer with HfO₂ deposition on microporous layer. Reprinted from [223], Copyright (2021), with permission from Elsevier. (c) Al₂O₃ coated Nafion membrane with increased mechanical strength. Reprinted from [224], Copyright (2015), with permission from Elsevier.

and suppressed electrochemical Ostwald ripening for uniform PtZn intermetallic nanocrystals.

Since the deactivation of Pt catalysts is resulted by the agglomeration, coalescence and Ostwald ripening of nanoparticles due to the dissolution of surface Pt atoms and weak interaction between Pt and supports, surface overcoating engineering is widely investigated to develop advanced electrocatalysts [203]. ALD has been utilized to modify the surface of Pt nanoparticles and carbon support materials due to the precise thickness control of overcoatings. In order to satisfy the work condition of hydrogen fuel cell, some metal oxides and nitrides with high corrosion resistance under acidic and oxidizing conditions have been chosen as overcoatings, such as TiO₂, ZrO₂, SnO₂ and WN. For instance, ultrathin TiO₂ was coated on Pt/C catalysts by ALD, which could achieve a good balance between the durability and activity by controlling the thickness of TiO₂ overcoating [204–206]. Liu *et al* achieved the stabilization of Pt low-coordinated sites on a commercial Pt/C catalyst by nitrogen doped TiO₂ by coupling selective ALD of TiO₂ and following nitrogen doping process [207]. With good conductivity and corrosion resistance, SnO₂ and WN coatings were also performed to increase the durability of Pt/C catalysts by mitigating the migration and agglomeration of Pt nanoparticles [208, 209]. As shown in figure 9(c), Lim *et al* prepared ZrO₂ coating on Pt catalysts with different ALD cycles, which were confirmed to be porous or to have a thickness of several nanometers or less [201]. MEA durability tests showed that 2 ALD cycles of ZrO₂ coating decreased the deterioration rate to one-fourth of that of the pure Pt catalyst, with a minor decrease in the fuel cell power. In order to protect the surface of Pt from coated metal oxide, Sun *et al* demonstrated an approach to stabilized Pt catalysts for ORR by area selective ALD of ZrO₂ and TaO_x, which was assisted by the blocking agent of oleylamine preventing the attachment of Zr and Ta precursors on Pt nanoparticles

[210, 211]. Besides Pt nanoparticles, the modifications of supports have also been investigated to improve the corrosion resistance of supports and enhance the interaction between Pt and supports. For instance, Tammeveski *et al* decorated acid-treated multi-walled carbon nanotubes by TiO₂ that exhibited strong metal-support interaction with subsequently deposited Pt nanoparticles [212, 213]. As shown in figure 9(d), Zhang *et al* prepared Al based coatings with enriched pores on nitrogen-doped carbon nanotubes via MLD, which was effective stabilizer for anchoring the Pt nanoparticles [202]. They also deposited highly dispersed nitrogen doped Ta₂O₅ nanoparticles on carbon black supports to prevent Pt nanocrystals from migration and aggregation [214].

4.3. MEA modification by ALD

In the MEA level, the performance of hydrogen fuel cell is not only related to the activity and stability of Pt catalysts, but also attributed to the electron and proton conductivity, the mass transport of gas reactants and management of water. The catalyst layer composed by supported Pt catalysts and ionomer is the key component for electrochemical reaction of reactants, where the nanostructure and distribution of ionomer are important for mass transport. As shown in figure 10(a), Sabarirajan *et al* designed and prepared a Pt nanoelectrode array for hydrogen fuel cell [215]. The Pt nanoelectrode array was prepared by Pt ALD onto anodized aluminium oxide discs with subsequently etching process, which was used as an ionomer-free electrode for transport and reaction kinetics studies, indicating the surface migration mechanism for proton transport. Bottom-up fabrication of cathode electrodes for ORR was developed with ALD technology to improve the Pt catalyst-ionomer interface and accelerate mass transport [216, 217]. Furthermore, an anode catalyst layer was prepared by directly depositing Pt nanoparticles with uniform size on gas

diffusion layer, which exhibited excellent activity and stability compared with the anode prepared using commercial carbon supported Pt catalysts and a conventional screen printing method [218, 219]. Although ALD was a powerful technique to prepare highly dispersed Pt catalysts on supports as presented above, Weimer *et al* found that the residual functional groups after Pt ALD could decrease the hydrophobicity of catalyst layer, which resulted in the poor MEA performance by inducing water flooding [220, 221]. They modified Pt/C catalysts by sub-monolayer WN films and subsequently thermal treatment that improved the catalyst performance in the mass transport region. ALD was employed to maintain MEA with a satisfactory water content and distribution. For instance, ultrathin layer of hydrophilic TiO₂ was coated on hydrophobic microporous layer of gas diffusion layer at the cathode, which resulted in high MEA performance at low humidity operation [222]. As shown in figure 10(b), different numbers of HfO₂ ALD cycle were used to modify the microporous layer on gas diffusion layer, which could control the water contact angle [223]. 25 ALD cycles of HfO₂ exhibited the smallest charge transfer resistance and mass transport resistance in low and high humidity conditions. As the widely used proton conducting media, Nafion membrane was coated by Al₂O₃ ALD to improve the mechanical strength and decrease the membrane permeability to gas reactants (figure 10(c)) [224]. The above achieved progresses indicate that the modifications of functional components in MEA by ALD are critical for the application of hydrogen fuel cell.

5. ALD reactors for catalytic and energy materials

ALD has been demonstrated to play an important role in designing and preparing advanced catalytic and energy materials by atomically precise controlling the surface and interface structures. Compared with conventional liquid and solid processes for surface coating or modification, ALD exhibits the advantages of high-precise control of coating thickness, good uniformity and conformality, as well as strong adhesion between coatings and substrates due to the characteristic of self-limiting chemical reaction. Nevertheless, as mentioned in previous section, the catalysts and electrode materials in batteries are powder materials with high specific surface areas, which suffer from particle agglomeration problem, much slow diffusion of precursors in agglomerates and lower deposition rate than that on planar substrates. Furthermore, the popularization of eco-friendly vehicles requires large amounts of catalytic and energy materials that ranges from tons to 10 000 tons. High mass production reactors with low cost ALD processes are the key to meet the practicality of powder ALD for industrialization. Based on conventional ALD reactors, lab scale powder ALD was usually performed by uniformly spreading powder on a tray that was just capable of coating grams of powder [225]. As shown in figure 11(a), the static powder bed with height large than 1 mm was loaded in a powder tray that incorporated in a viscous flow ALD reactor, which required much longer dose and pure times to ensure adequate penetration of precursors. In order to monitor the reaction processes

during ALD, Naumann d' Stempel *et al* integrated a magnetically suspended balance in fixed-bed reactor to record the mass changes of powder [226]. Recently, a fixed-bed ALD reactor was used to prepare Ni catalysts on mesoporous ZrO₂ supports [227]. The precursors and inert gas were led downwards through the fixed bed with 5 g of ZrO₂ supports and an ALD cycle needs several hours. To address the limitation of precursor diffusion in static powder bed, various methods have been reported previously to disperse powder by overcoming the interparticle cohesion, such as fluidization, rotation and vibration [228–230]. Compared with static bed ALD reactor, larger quantities of powder can be coated in these ALD reactors with shorter precursor dose and purge times. For instance, Lu *et al* performed Al₂O₃ ALD on 10 g of Pt/SiO₂ catalyst in a commercial fluidized bed reactor [231]. By *in situ* monitoring the surface reactions of ALD, the optimized precursor dose times for trimethylaluminum and water were 28 min and 17 min, respectively, while the precursor utilization of trimethylaluminum was $91.8 \pm 14.6\%$.

In order to promote the industrialization of powder ALD, much attention has been paid to developing new powder ALD reactors to further increase the mass production and coating efficiency. Increasing the volume of reactor was a direct strategy to increase the throughput based on previously reported fluidized bed reactor or rotary reactor, while the corresponding ALD processes should also be optimized. As shown in figure 11(a), high-capacity rotary drum was inserted into a viscous-flow tubular ALD reactor, which can provide homogeneous coating on tens of grams of powder with less than 2 min saturation of trimethylaluminum [232, 233]. A rotary reactor was incorporated with a moveable dual-zone furnace to change the temperature of powder for precursor adsorption and oxidative removal of the precursor ligands, which can coat a large quantity of powder with high specific surface area in a relatively short period of time [234]. The disperse powder bed coupled with external force field was another strategy to increase the mass production and coating efficiency by enhancing the gas-solid contact between precursors and powder. As shown in figure 11(b), Duan *et al* designed a fluidized bed coupled rotary reactor for powder ALD [235]. The double-layer powder cartridge can ensure precursors flowing through the particle bed exclusively to achieve high utilization without static exposure operation. Recently, they reported an ultrasonic vibration-assisted fluidized bed ALD reactor to promote the deagglomeration of powder and facilitate the heat transfer and precursor diffusion in high-volume powder bed (figure 11(c)) [236]. Different with the batchwise operation of fluidized bed or rotary reactors, spatial ALD was also applied for powder coating to achieve the continuous operation. A high-throughput semi-continuous ALD system was developed by connecting several fluidized bed reactors and feeding powder on the one side and removing them at the other side, which can achieve the production of hundreds of kilograms of powder [130]. As shown in figure 11(d), van Ommen *et al* designed a lab-scale pneumatic transport reactor for spatial powder ALD that deposited Pt nanoclusters on TiO₂ supports with a production rate of 1 g min^{-1} [237]. Based on the linear vibration to convey particles through alternating

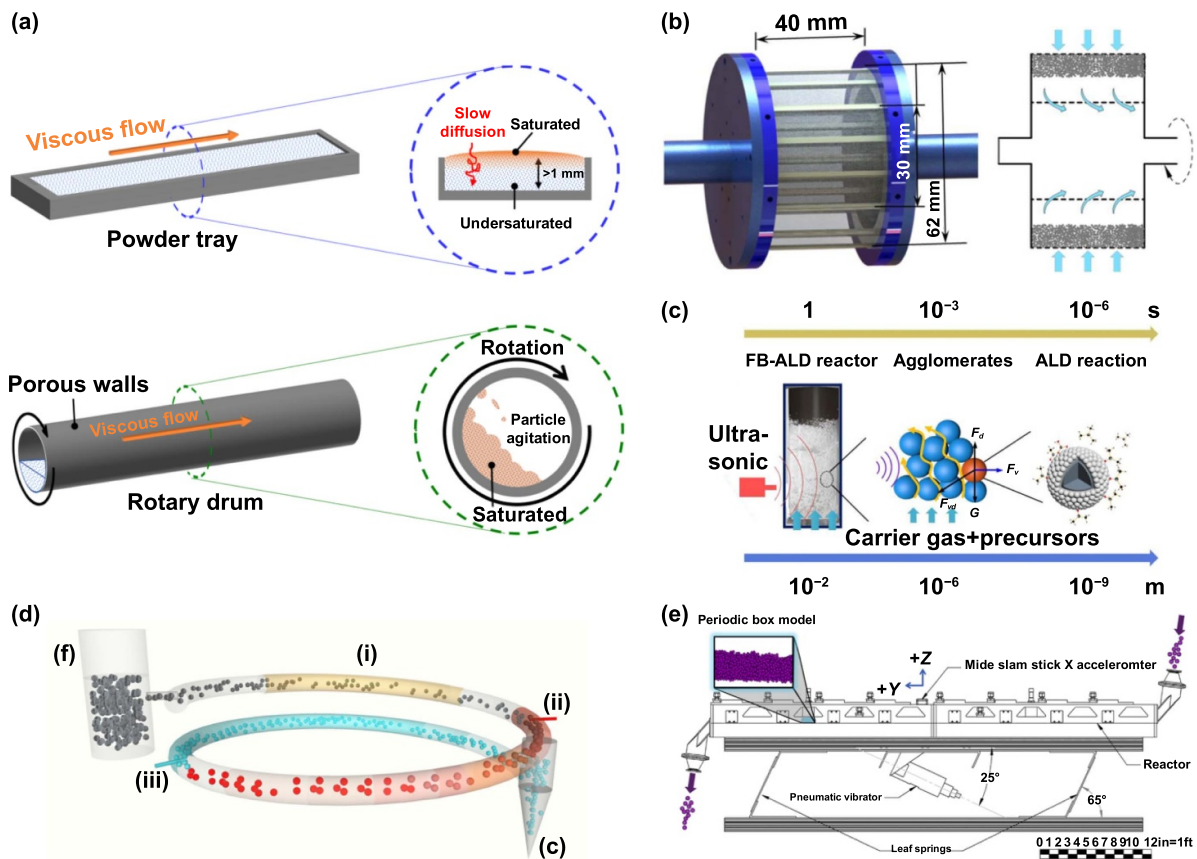


Figure 11. ALD reactors for catalytic and energy materials. (a) Viscous flow reactor with a stainless-steel tray or high-capacity rotary drum for powder ALD. Reproduced with permission from [232]. (b) Particle cartridge of a fluidization coupled rotary ALD reactor. Reprinted from [235], with the permission of AIP Publishing. (c) High-volume powder ALD by ultrasonic vibration-assisted fluidized bed. Reproduced from [236]. © 2022 The Author(s). Published by IOP Publishing Ltd on behalf of the IMMT. CC BY 4.0. (d) Pneumatic transport reactor for spatial powder ALD. Reproduced with permission from [237]. (e) Continuous vibrating bed reactor for spatial powder ALD. Reprinted from [238], Copyright (2021), with permission from Elsevier.

regions of precursor gas, a continuous vibrating bed reactor was developed for spatial powder ALD, the powder flow behavior in which can be controlled by adjusting the frequency and amplitude of excitation waveform for horizontal conveyors. (figure 11(e)) [238]. Besides spatial powder ALD, the porous electrodes or separator can also be directly modified by spatial ALD, which is more compatible with the flow line production [239, 240]. Much longer precursor exposure time was required for the diffusion of precursors in porous structures, which limited the moving speed of electrodes or separator [241, 242]. Furthermore, the uniformity of precursor distribution in the width direction and the utilization of precursor could be further optimized by developing the ALD reactors and processes.

6. Summary and perspectives

In this review, recent progress of ALD on the controllable preparation and modification of advanced catalytic and energy materials, as well as their enhanced performance for exhaust emission control, power lithium ion battery and hydrogen fuel cell have been summarized and discussed. The low

temperature activity of supported metal and oxide catalysts are improved by controlling their nucleation, size and distribution, as well as the metal-support interactions, while the promising strategies by encapsulating Pt-based nanoparticles in ALD deposited overlayers are developed to enhance the sintering resistance under high temperature conditions of exhaust emission control system. ALD has also been performed to prepare and modify highly dispersed Pt catalysts and conductive supports to enhance the intrinsic catalytic activity and stability for cathode ORR in hydrogen fuel cell. For power lithium ion battery, the ALD coatings with controllable thickness on cathode, anode and separator cannot only improve the electrochemical and structural stability by suppressing undesirable side reactions during charge–discharge cycling, but also ensure the transport of electrons and Li ions to keep the discharge capacity and rate performance. The electron and proton conductivity, as well as the mass transport of gas reactants of MEA are enhanced by ALD modifying the functional components, such as catalyst layer, gas diffusion layer and proton exchange membrane.

Although ALD has been applied to enhance the chemical and electrochemical performance of catalytic and energy materials for exhaust emission control, power lithium ion

battery and hydrogen fuel cell, there are still several challenges that involved in the research and development of ALD on the future practical applications for eco-friendly vehicles. One of the challenges is the development of new precursors. For instance, the cost of precursors should be decreased for large-scale applications of ALD, especially for the expensive precious metal precursors. At present, metal oxides are the most common materials for ALD overcoatings on catalytic and energy materials. New precursors with high chemical activity and the corresponding ALD processes for other metal compounds such as carbides, nitrides are also important for the performance enhancement of catalytic and energy materials. Furthermore, much attention needs to be paid to the performance evaluation of ALD modified materials in practical device level. For instance, the performance of oxide supported Pt group metal catalysts for three-way catalysis or diesel oxidation catalysis can be evaluated under the practical reaction atmosphere and gas hourly space velocity condition. Pouch cell is needed to study the effect of ALD coatings on cathode or anode materials for lithium ion battery, while the electrochemical performance of modified MEA can be evaluated by hydrogen fuel cell stack under dynamic cycle working condition.

Large-scale and efficient production of ALD modified materials is also a challenge for the practical applications. For rotary ALD reactor, the production rate is closely dependent on the volume of rotary drum, which is usually reported less than hundreds of grams of powder per batch. When fluidized ALD reactor is coupled with external force field, such as mechanical vibration, rotation and ultrasound, the production rate can reach to hundreds of kilograms of powder per batch due to the promoted disaggregation and uniform distribution of catalysts or cathode/anode particles. However, the production volume still cannot satisfy the requirement of tons of materials per year in industrial applications. In order to further increase the production volume of powder ALD, the comprehensive reaction mechanism and kinetics of ALD in dynamic agglomerates in fluidized bed should be studied. The diffusion and reaction kinetics model of precursor in dynamic agglomerates should be developed to investigate the effect of external force field on ALD process on particles, which can give guidance to reactor design and ALD parameters optimization. Furthermore, large amounts of precursors need to be delivered into reactor for mass production of particles, which should be quantitative and concentration controllable. *In situ* monitoring of reaction process of ALD is necessary to be coupled to control the supply of precursors and balance the reaction efficiency and precursor utilization. Spatial ALD is a promising technique to achieve mass production, which can not only be applied on particle coatings, but also continuously deposit materials on flexible electrode or separator. Since the diffusion and reaction of precursors in porous substrate is much slow than that on planar substrate, the moving speed of porous substrate should be compatible with industrial flow line production by designing highly efficient and uniform injector for precursor distribution. Above all, the powder and spatial ALD reactors, as well as the corresponding ALD processes are of great significance to scale up the manufacturing process by increasing the deposition efficiency and precursor utilization,

which can facilitate the industrialization of ALD for advanced catalytic and energy materials.

Acknowledgments

This study was supported by the National Key R&D Program of China (2020YFB2010401 and 2022YFF1500400), National Natural Science Foundation of China (51835005 and 52271216), Hubei Province Natural Science Foundation for Innovative Research Group (2020CFA030), Fundamental Research Funds for the Central Universities, HUST (2020kfyXJJS100) and Tencent Foundation. The authors acknowledge the technology support from the Analytic Testing Center and Flexible Electronics Research Center.

ORCID iD

Rong Chen  <https://orcid.org/0000-0001-7371-1338>

References

- [1] Datye A K and Votsmeier M 2021 Opportunities and challenges in the development of advanced materials for emission control catalysts *Nat. Mater.* **20** 1049–59
- [2] Du J Y, Ouyang M G and Chen J F 2017 Prospects for Chinese electric vehicle technologies in 2016–2020: ambition and rationality *Energy* **120** 584–96
- [3] Wagner F T, Lakshmanan B and Mathias M F 2010 Electrochemistry and the future of the automobile *J. Phys. Chem. Lett.* **1** 2204–19
- [4] Luo Y, Wu Y H, Li B, Mo T D, Li Y, Feng S P, Qu J K and Chu P K 2021 Development and application of fuel cells in the automobile industry *J. Energy Storage* **42** 103124
- [5] Wang J Y, Wang H L and Fan Y 2018 Techno-economic challenges of fuel cell commercialization *Engineering* **4** 352–60
- [6] Beniya A and Higashi S 2019 Towards dense single-atom catalysts for future automotive applications *Nat. Catal.* **2** 590–602
- [7] Zubi G, Dufo-López R, Carvalho M and Pasaoglu G 2018 The lithium-ion battery: state of the art and future perspectives *Renew. Sustain. Energy Rev.* **89** 292–308
- [8] Zeng X Q, Li M, El-Hady D A, Alshitari W, Al-Bogami A S, Lu J and Amine K 2019 Commercialization of lithium battery technologies for electric vehicles *Adv. Energy Mater.* **9** 1900161
- [9] Debe M K 2012 Electrocatalyst approaches and challenges for automotive fuel cells *Nature* **486** 43–51
- [10] Yoshida T and Kojima K 2015 Toyota MIRAI fuel cell vehicle and progress toward a future hydrogen society *Electrochem. Soc. Interface* **24** 45–49
- [11] Nie L *et al* 2017 Activation of surface lattice oxygen in single-atom Pt/CeO₂ for low-temperature CO oxidation *Science* **358** 1419–23
- [12] Liu L C and Corma A 2018 Metal catalysts for heterogeneous catalysis: from single atoms to nanoclusters and nanoparticles *Chem. Rev.* **118** 4981–5079
- [13] Ren X F, Wang Y R, Liu A M, Zhang Z H, Lv Q Y and Liu B H 2020 Current progress and performance improvement of Pt/C catalysts for fuel cells *J. Mater. Chem. A* **8** 24284–306
- [14] Wang X X, Swihart M T and Wu G 2019 Achievements, challenges and perspectives on cathode catalysts in proton

- exchange membrane fuel cells for transportation *Nat. Catal.* **2** 578–89
- [15] Lambert C K 2019 Current state of the art and future needs for automotive exhaust catalysis *Nat. Catal.* **2** 554–7
- [16] Feng X N, Ren D S, He X M and Ouyang M G 2020 Mitigating thermal runaway of lithium-ion batteries *Joule* **4** 743–70
- [17] Ding Y, Mu D B, Wu B R, Wang R, Zhao Z K and Wu F 2017 Recent progresses on nickel-rich layered oxide positive electrode materials used in lithium-ion batteries for electric vehicles *Appl. Energy* **195** 586–99
- [18] Kodama K, Nagai T, Kuwaki A, Jinnouchi R and Morimoto Y 2021 Challenges in applying highly active Pt-based nanostructured catalysts for oxygen reduction reactions to fuel cell vehicles *Nat. Nanotechnol.* **16** 140–7
- [19] Stamenkovic V R, Strmcnik D, Lopes P P and Markovic N M 2017 Energy and fuels from electrochemical interfaces *Nat. Mater.* **16** 57–69
- [20] Zhang J M, Li Y C, Cao K and Chen R 2022 Advances in atomic layer deposition *Nanomanuf. Metrol.* **5** 191–208
- [21] Suntola T and Antson J 1977 Method for producing compound thin films *U. S. Patent. No.* 4,058,430
- [22] George S M 2010 Atomic layer deposition: an overview *Chem. Rev.* **110** 111–31
- [23] Johnson R W, Hultqvist A and Bent S F 2014 A brief review of atomic layer deposition: from fundamentals to applications *Mater. Today* **17** 236–46
- [24] Chen R, Li Y C, Cai J M, Cao K and Lee H B R 2020 Atomic level deposition to extend Moore's law and beyond *Int. J. Extreme Manuf.* **2** 022002
- [25] Gray J M, Houlton J P, Gertsch J C, Brown J J, Rogers C T, George S M and Bright V M 2014 Hemispherical micro-resonators from atomic layer deposition *J. Micromech. Microeng.* **24** 125028
- [26] Ives R L, Oldham C J, Daubert J S, Gremaud A P, Collins G, Marsden D, Bui T, Fusco M A, Mitsdarffer B and Parsons G N 2018 Corrosion mitigation coatings for RF sources and components *IEEE Trans. Electron Devices* **65** 2385–92
- [27] Lin Y C, Chung V P J, Santhanam S, Mukherjee T and Fedder G K 2020 Sidewall metallization on CMOS MEMS by platinum ALD patterning *J. Microelectromech. Syst.* **29** 978–83
- [28] Wooding J P, Li Y, Kalaitzidou K and Losego M D 2020 Engineering the interfacial chemistry and mechanical properties of cellulose-reinforced epoxy composites using atomic layer deposition (ALD) *Cellulose* **27** 6275–85
- [29] Rodríguez R E, Lee T H, Chen Y X, Kazyak E, Huang C, Cho T H, LePage W S, Thouless M D, Banu M and Dasgupta N P 2021 Electrically conductive kevlar fibers and polymer-matrix composites enabled by atomic layer deposition *ACS Appl. Polym. Mater.* **3** 5959–68
- [30] Mousa M B M, Oldham C J and Parsons G N 2015 Precise nanoscale surface modification and coating of macroscale objects: open-environment in loco atomic layer deposition on an automobile *ACS Appl. Mater. Interfaces* **7** 19523–9
- [31] Niu W B, Zhang L L, Wang Y P and Zhang S F 2019 Multicolored one-dimensional photonic crystal coatings with excellent mechanical robustness, strong substrate adhesion, and liquid and particle impalement resistance *J. Mater. Chem. C* **7** 3463–70
- [32] Gupta B, Hossain A, Riaz A, Sharma A, Zhang D D, Tan H H, Jagadish C, Catchpole K, Hoex B and Karuturi S 2022 Recent advances in materials design using atomic layer deposition for energy applications *Adv. Funct. Mater.* **32** 2109105
- [33] Gandla D and Tan D Q 2019 Progress report on atomic layer deposition toward hybrid nanocomposite electrodes for next generation supercapacitors *Adv. Mater. Interfaces* **6** 1900678
- [34] Zhao Z, Huang G S, Kong Y, Cui J Z, Solovov A A, Li X F and Mei Y F 2022 Atomic layer deposition for electrochemical energy: from design to industrialization *Electrochem. Energy Rev.* **5** 31
- [35] Li Z D, Su J J and Wang X D 2021 Atomic layer deposition in the development of supercapacitor and lithium-ion battery devices *Carbon* **179** 299–326
- [36] Liu H Z, Zhang G H, Zheng X, Chen F J and Duan H G 2020 Emerging miniaturized energy storage devices for microsystem applications: from design to integration *Int. J. Extreme Manuf.* **2** 042001
- [37] Lv Z S, Li W L, Wei J Q, Ho F, Cao J and Chen X D 2023 Autonomous chemistry enabling environment-adaptive electrochemical energy storage devices *CCS Chem.* **5** 11–29
- [38] Chen R, Shan B, Liu X and Cao K 2020 Catalysts via atomic layer deposition *Recent Advances in Nanoparticle Catalysis* ed P W N M Van Leeuwen and C Claver (Cham: Springer) pp 69–105
- [39] Li Z S, Li J W, Liu X and Chen R 2021 Progress in enhanced fluidization process for particle coating via atomic layer deposition *Chem. Eng. Process. Process Intensif.* **159** 108234
- [40] Longrie D, Deduytsche D and Detavernier C 2014 Reactor concepts for atomic layer deposition on agitated particles: a review *J. Vac. Sci. Technol. A* **32** 010802
- [41] Adhikari S, Selvaraj S and Kim D H 2018 Progress in powder coating technology using atomic layer deposition *Adv. Mater. Interfaces* **5** 1800581
- [42] Didden A P, Middelkoop J, Besling W F A, Nanu D E and van de Krol R 2014 Fluidized-bed atomic layer deposition reactor for the synthesis of core-shell nanoparticles *Rev. Sci. Instrum.* **85** 013905
- [43] Onn T M, Küngas R, Fornasiero P, Huang K and Gorte R J 2018 Atomic layer deposition on porous materials: problems with conventional approaches to catalyst and fuel cell electrode preparation *Inorganics* **6** 34
- [44] Weimer A W 2019 Particle atomic layer deposition *J. Nanopart. Res.* **21** 9
- [45] Van Bui H, Grillo F and van Ommen J R 2017 Atomic and molecular layer deposition: off the beaten track *Chem. Commun.* **53** 45–71
- [46] Hu Y Y, Lu J and Feng H 2021 Surface modification and functionalization of powder materials by atomic layer deposition: a review *RSC Adv.* **11** 11918–42
- [47] Parsons G N, Elam J W, George S M, Haukka S, Jeon H, Kessels W M M, Leskelä M, Poodt P, Ritala M and Rosnagel S M 2013 History of atomic layer deposition and its relationship with the American Vacuum Society *J. Vac. Sci. Technol. A* **31** 050818
- [48] O'Neill B J, Jackson D H K, Lee J, Canlas C, Stair P C, Marshall C L, Elam J W, Kuech T F, Dumesic J A and Huber G W 2015 Catalyst design with atomic layer deposition *ACS Catal.* **5** 1804–25
- [49] Cao K, Cai J M, Liu X and Chen R 2018 Review Article: catalysts design and synthesis via selective atomic layer deposition *J. Vac. Sci. Technol. A* **36** 010801
- [50] Jung Y S, Cavanagh A S, Gedvilas L, Widjonarko N E, Scott I D, Lee S H, Kim G H, George S M and Dillon A C 2012 Improved functionality of lithium-ion batteries enabled by atomic layer deposition on the porous microstructure of polymer separators and coating electrodes *Adv. Energy Mater.* **2** 1022–7
- [51] Elam J W, Dasgupta N P and Prinz F B 2011 ALD for clean energy conversion, utilization, and storage *MRS Bull.* **36** 899–906

- [52] Lee M J *et al* 2022 Powder coatings via atomic layer deposition for batteries: a review *Chem. Mater.* **34** 3539–87
- [53] Wang C L, Gu X K, Yan H, Lin Y, Li J J, Liu D D, Li W X and Lu J L 2017 Water-mediated Mars-Van Krevelen mechanism for CO oxidation on ceria-supported single-atom Pt₁ catalyst *ACS Catal.* **7** 887–91
- [54] Ye X X, Wang H W, Lin Y, Liu X Y, Cao L N, Gu J and Lu J L 2019 Insight of the stability and activity of platinum single atoms on ceria *Nano Res.* **12** 1401–9
- [55] Liu X, Jia S F, Yang M, Tang Y T, Wen Y W, Chu S Q, Wang J B, Shan B and Chen R 2020 Activation of subnanometric Pt on Cu-modified CeO₂ via redox-coupled atomic layer deposition for CO oxidation *Nat. Commun.* **11** 4240
- [56] Hoang S, Lu X X, Tang W X, Wang S B, Du S C, Nam C Y, Ding Y, Vinluan III R D, Zheng J and Gao P X 2019 High performance diesel oxidation catalysts using ultra-low Pt loading on titania nanowire array integrated cordierite honeycombs *Catal. Today* **320** 2–10
- [57] Tang W X, Lu X X, Liu F Y, Du S C, Weng J F, Hoang S, Wang S B, Nam C Y and Gao P X 2019 Ceria-based nanoflake arrays integrated on 3D cordierite honeycombs for efficient low-temperature diesel oxidation catalyst *Appl. Catal. B* **245** 623–34
- [58] Li J H, Liang X H, King D M, Jiang Y B and Weimer A W 2010 Highly dispersed Pt nanoparticle catalyst prepared by atomic layer deposition *Appl. Catal. B* **97** 220–6
- [59] Enterkin J A, Setthapun W, Elam J W, Christensen S T, Rabuffetti F A, Marks L D, Stair P C, Poepfelmeier K R and Marshall C L 2011 Propane oxidation over Pt/SrTiO₃ nanocuboids *ACS Catal.* **1** 629–35
- [60] Chen B R *et al* 2018 Morphology and CO oxidation activity of Pd nanoparticles on SrTiO₃ nanopolyhedra *ACS Catal.* **8** 4751–60
- [61] Liu X, Tang Y T, Shen M Q, Li W, Chu S Q, Shan B and Chen R 2018 Bifunctional CO oxidation over Mn-mullite anchored Pt sub-nanoclusters via atomic layer deposition *Chem. Sci.* **9** 2469–73
- [62] Zuo Y Q *et al* 2022 Synthesis of a spatially confined, highly durable, and fully exposed Pd cluster catalyst via sequential site-selective atomic layer deposition *ACS Appl. Mater. Interfaces* **14** 14466–73
- [63] Onn T M, Zhang S Y, Arroyo-Ramirez L, Xia Y, Wang C, Pan X Q, Graham G W and Gorte R J 2017 High-surface-area ceria prepared by ALD on Al₂O₃ support *Appl. Catal. B* **201** 430–7
- [64] Mao X Y, Foucher A, Stach E A and Gorte R J 2019 A study of support effects for CH₄ and CO oxidation over Pd catalysts on ALD-modified Al₂O₃ *Catal. Lett.* **149** 905–15
- [65] Onn T M, Dai S, Chen J Y, Pan X Q, Graham G W and Gorte R J 2017 High-surface area ceria-zirconia films prepared by atomic layer deposition *Catal. Lett.* **147** 1464–70
- [66] Mao X Y, Foucher A C, Montini T, Stach E A, Fornasiero P and Gorte R J 2020 Epitaxial and strong support interactions between Pt and LaFeO₃ films stabilize Pt dispersion *J. Am. Chem. Soc.* **142** 10373–82
- [67] Lin C, Foucher A C, Ji Y C, Curran C D, Stach E A, McIntosh S and Gorte R J 2019 “Intelligent” Pt catalysts studied on high-surface-area CaTiO₃ films *ACS Catal.* **9** 7318–27
- [68] Mao X Y, Foucher A C, Stach E A and Gorte R J 2019 “Intelligent” Pt catalysts based on thin LaCoO₃ films prepared by atomic layer deposition *Inorganics* **7** 113
- [69] Onn T M, Monai M, Dai S, Fonda E, Montini T, Pan X Q, Graham G W, Fornasiero P and Gorte R J 2018 Smart Pd catalyst with improved thermal stability supported on high-surface-area LaFeO₃ prepared by atomic layer deposition *J. Am. Chem. Soc.* **140** 4841–8
- [70] Duan H M, You R, Xu S T, Li Z R, Qian K, Cao T, Huang W X and Bao X H 2019 Pentacoordinated Al³⁺-stabilized active Pd structures on Al₂O₃-coated palladium catalysts for methane combustion *Angew. Chem. Int. Ed.* **58** 12043–8
- [71] Cui W H, Li S D, Wang D D, Deng Y Z and Chen Y F 2019 High reactivity and sintering resistance of CH₄ oxidation over modified Pd/Al₂O₃ *Catal. Commun.* **119** 86–90
- [72] Liang X H, Li J H, Yu M, McMurray C N, Falconer J L and Weimer A W 2011 Stabilization of supported metal nanoparticles using an ultrathin porous shell *ACS Catal.* **1** 1162–5
- [73] Onn T M, Zhang S Y, Arroyo-Ramirez L, Chung Y C, Graham G W, Pan X Q and Gorte R J 2015 Improved thermal stability and methane-oxidation activity of Pd/Al₂O₃ catalysts by atomic layer deposition of ZrO₂ *ACS Catal.* **5** 5696–701
- [74] Onn T M, Arroyo-Ramirez L, Monai M, Oh T S, Talati M, Fornasiero P, Gorte R J and Khader M M 2016 Modification of Pd/CeO₂ catalyst by atomic layer deposition of ZrO₂ *Appl. Catal. B* **197** 280–5
- [75] Lee S, Lin C, Kim S, Mao X Y, Kim T, Kim S J, Gorte R J and Jung W 2021 Manganese oxide overlayers promote CO oxidation on Pt *ACS Catal.* **11** 13935–46
- [76] Liu X, Zhu Q Q, Lang Y, Cao K, Chu S Q, Shan B and Chen R 2017 Oxide-nanotrap-anchored platinum nanoparticles with high activity and sintering resistance by area-selective atomic layer deposition *Angew. Chem. Int. Ed.* **56** 1648–52
- [77] Cao K, Shi L, Gong M, Cai J M, Liu X, Chu S Q, Lang Y, Shan B and Chen R 2017 Nanofence stabilized platinum nanoparticles catalyst via facet-selective atomic layer deposition *Small* **13** 1700648
- [78] Cai J M, Zhang J, Cao K, Gong M, Lang Y, Liu X, Chu S Q, Shan B and Chen R 2018 Selective passivation of Pt nanoparticles with enhanced sintering resistance and activity toward CO oxidation via atomic layer deposition *ACS Appl. Nano Mater.* **1** 522–30
- [79] Wang X F, Jin B T, Jin Y, Wu T P, Ma L and Liang X H 2020 Supported single Fe atoms prepared via atomic layer deposition for catalytic reactions *ACS Appl. Nano Mater.* **3** 2867–74
- [80] Han S W, Kim D H, Jeong M G, Park K J and Kim Y D 2016 CO oxidation catalyzed by NiO supported on mesoporous Al₂O₃ at room temperature *Chem. Eng. J.* **283** 992–8
- [81] Jackson D H K, Schwartz M M, Ngo C, Facticeau D, Pylypenko S, Marshall C L and Dameron A A 2019 Hydrocarbon catalyzed-selective catalytic reduction catalysts using core-shell atomic layer deposited CeO₂ and ZrO₂ *J. Vac. Sci. Technol. A* **37** 020919
- [82] Shen J and Hess C 2020 High surface area VO_x/TiO₂/SBA-15 model catalysts for ammonia SCR prepared by atomic layer deposition *Catalysts* **10** 1386
- [83] Sun L W, Li K, Zhang Z S, Hu X F, Tian H Y, Zhang Y B and Yang X G 2019 MnO₂-Graphene-oxide-scroll-TiO₂ composite catalyst for low-temperature NH₃-SCR of NO with good steam and SO₂ resistance obtained by low-temperature carbon-coating and selective atomic layer deposition *Catal. Sci. Technol.* **9** 1602–8
- [84] Tian H Y, Ping Y, Zhang Y B, Zhang Z S, Sun L W, Liu P, Zhu J J and Yang X G 2021 Atomic layer deposition of silica to improve the high-temperature hydrothermal stability of Cu-SSZ-13 for NH₃ SCR of NO_x *J. Hazard. Mater.* **416** 126194
- [85] Qi X R, Han L P, Deng J, Lan T W, Wang F L, Shi L Y and Zhang D S 2022 SO₂-tolerant catalytic reduction of NO_x

- via tailoring electron transfer between surface iron sulfate and subsurface ceria *Environ. Sci. Technol.* **56** 5840–8
- [86] Ivanova T V, Toivonen J, Maydannik P S, Kääriäinen T, Sillanpää M, Homola T and Cameron D C 2016 Atomic layer deposition of cerium oxide for potential use in diesel soot combustion *J. Vac. Sci. Technol. A* **34** 031506
- [87] Ivanova T V, Homola T, Bryukvin A and Cameron D C 2018 Catalytic performance of Ag₂O and Ag doped CeO₂ prepared by atomic layer deposition for diesel soot oxidation *Coatings* **8** 237
- [88] Mackus A J M, Weber M J, Thissen N F W, Garcia-Alonso D, Vervuurt R H J, Assali S, Bol A A, Verheijen M A and Kessels W M M 2016 Atomic layer deposition of Pd and Pt nanoparticles for catalysis: on the mechanisms of nanoparticle formation *Nanotechnology* **27** 034001
- [89] Gould T D, Lubers A M, Corpuz A R, Weimer A W, Falconer J L and Medlin J W 2015 Controlling nanoscale properties of supported platinum catalysts through atomic layer deposition *ACS Catal.* **5** 1344–52
- [90] Yan H *et al* 2017 Bottom-up precise synthesis of stable platinum dimers on graphene *Nat. Commun.* **8** 1070
- [91] Lu J L 2022 Atomic lego catalysts synthesized by atomic layer deposition *Acc. Mater. Res.* **3** 358–68
- [92] Li X *et al* 2022 Functional CeO_x nanoglues for robust atomically dispersed catalysts *Nature* **611** 284–8
- [93] Xie S H *et al* 2022 Pt atomic single-layer catalyst embedded in defect-enriched ceria for efficient CO oxidation *J. Am. Chem. Soc.* **144** 21255–66
- [94] Lu Y B, Zhang Z H, Lin F, Wang H M and Wang Y 2020 Single-atom automobile exhaust catalysts *ChemNanoMat* **6** 1659–82
- [95] Jones J *et al* 2016 Thermally stable single-atom platinum-on-ceria catalysts via atom trapping *Science* **353** 150–4
- [96] Yan D X, Chen J and Jia H P 2020 Temperature-induced structure reconstruction to prepare a thermally stable single-atom platinum catalyst *Angew. Chem. Int. Ed.* **59** 13562–7
- [97] Jeong H, Kwon O, Kim B S, Bae J, Shin S, Kim H E, Kim J and Lee H 2020 Highly durable metal ensemble catalysts with full dispersion for automotive applications beyond single-atom catalysts *Nat. Catal.* **3** 368–75
- [98] Kim C H, Qi G S, Dahlberg K and Li W 2010 Strontium-doped perovskites rival platinum catalysts for treating NO_x in simulated diesel exhaust *Science* **327** 1624–7
- [99] Wang W C *et al* 2012 Mixed-phase oxide catalyst based on Mn-mullite (Sm, Gd)Mn₂O₅ for NO oxidation in diesel exhaust *Science* **337** 832–5
- [100] Chen Z Z, Liu X, Cho K, Chen R and Shan B 2015 Density functional theory study of the oxygen chemistry and NO oxidation mechanism on low-index surfaces of SmMn₂O₅ mullite *ACS Catal.* **5** 4913–26
- [101] Liu X, Yang J Q, Shen G R, Shen M Q, Zhao Y K, Cho K, Shan B and Chen R 2019 Tuning the structure of bifunctional Pt/SmMn₂O₅ interfaces for promoted low-temperature CO oxidation activity *Nanoscale* **11** 8150–9
- [102] Mao X Y, Lin C, Graham G W and Gorte R J 2020 A perspective on thin-film perovskites as supports for metal catalysts *ACS Catal.* **10** 8840–9
- [103] Lin C, Foucher A C, Ji Y C, Stach E A and Gorte R J 2020 Investigation of Rh-titanate (ATiO₃) interactions on high-surface-area perovskite thin films prepared by atomic layer deposition *J. Mater. Chem. A* **8** 16973–84
- [104] Lu J L, Liu B, Greeley J P, Feng Z X, Libera J A, Lei Y, Bedzyk M J, Stair P C and Elam J W 2012 Porous alumina protective coatings on palladium nanoparticles by self-poisoned atomic layer deposition *Chem. Mater.* **24** 2047–55
- [105] Lu J L, Fu B S, Kung M C, Xiao G M, Elam J W, Kung H H and Stair P C 2012 Coking- and sintering-resistant palladium catalysts achieved through atomic layer deposition *Science* **335** 1205–8
- [106] Lu J L and Stair P C 2010 Low-temperature ABC-type atomic layer deposition: synthesis of highly uniform ultrafine supported metal nanoparticles *Angew. Chem. Int. Ed.* **49** 2547–51
- [107] Canlas C P, Lu J L, Ray N A, Grosso-Giordano N A, Lee S, Elam J W, Winans R E, Van Duyne R P, Stair P C and Notestein J M 2012 Shape-selective sieving layers on an oxide catalyst surface *Nat. Chem.* **4** 1030–6
- [108] Piernavieja-Hermida M, Lu Z, White A, Low K B, Wu T P, Elam J W, Wu Z L and Lei Y 2016 Towards ALD thin film stabilized single-atom Pd₁ catalysts *Nanoscale* **8** 15348–56
- [109] Zhang S F *et al* 2022 Surface isolation of single metal complexes or clusters by a coating sieving layer via atomic layer deposition *Cell Rep. Phys. Sci.* **3** 100787
- [110] Wen Y W, Cai J M, Zhang J, Yang J Q, Shi L, Cao K, Chen R and Shan B 2019 Edge-selective growth of MCp₂ (M = Fe, Co, and Ni) precursors on Pt nanoparticles in atomic layer deposition: a combined theoretical and experimental study *Chem. Mater.* **31** 101–11
- [111] Yang J Q, Cao K, Hu Q, Wen Y W, Liu X, Chen R and Shan B 2020 Unravelling the selective growth mechanism of AlO_x with dimethylaluminum isopropoxide as a precursor in atomic layer deposition: a combined theoretical and experimental study *J. Mater. Chem. A* **8** 4308–17
- [112] Cai J M, Merckx M J M, Lan Y X, Jing Y, Cao K, Wen Y W, Kessels W M M, Mackus A J M and Chen R 2021 Dependence of inherent selective atomic layer deposition of FeO_x on Pt nanoparticles on the coreactant and temperature *J. Vac. Sci. Technol. A* **39** 012404
- [113] Gao Z and Qin Y 2017 Design and properties of confined nanocatalysts by atomic layer deposition *Acc. Chem. Res.* **50** 2309–16
- [114] Xu D *et al* 2017 Controllable deposition of Pt nanoparticles into a KL zeolite by atomic layer deposition for highly efficient reforming of n-heptane to aromatics *Catal. Sci. Technol.* **7** 1342–50
- [115] Gao Z, Dong M, Wang G Z, Sheng P, Wu Z W, Yang H M, Zhang B, Wang G F, Wang J G and Qin Y 2015 Multiply confined nickel nanocatalysts produced by atomic layer deposition for hydrogenation reactions *Angew. Chem. Int. Ed.* **54** 9006–10
- [116] Wang M H, Gao Z, Zhang B, Yang H M, Qiao Y, Chen S, Ge H B, Zhang J K and Qin Y 2016 Ultrathin coating of confined Pt nanocatalysts by atomic layer deposition for enhanced catalytic performance in hydrogenation reactions *Chem. Eur. J.* **22** 8438–43
- [117] Gao Y, Park J and Liang X H 2018 Synergic titanium nitride coating and titanium doping by atomic layer deposition for stable- and high-performance Li-Ion battery *J. Electrochem. Soc.* **165** A3871–7
- [118] Lee D S H, Im W B and Liang X H 2019 High density conductive LiFePO₄ cathode with enhanced high-rate and high temperature performance *Mater. Chem. Phys.* **232** 367–73
- [119] Jin Y, Yu H, He X Q and Liang X H 2022 Stabilizing the interface of all-solid-state electrolytes against cathode electrodes by atomic layer deposition *ACS Appl. Energy Mater.* **5** 760–9
- [120] Shi Y, Zhang M H, Qian D N and Meng Y S 2016 Ultrathin Al₂O₃ coatings for improved cycling performance and

- thermal stability of $\text{LiNi}_{0.5}\text{Co}_{0.2}\text{Mn}_{0.3}\text{O}_2$ cathode material *Electrochim. Acta* **203** 154–61
- [121] Zhao L N, Chen G R, Weng Y H, Yan T T, Shi L Y, An Z X and Zhang D S 2020 Precise Al_2O_3 coating on $\text{LiNi}_{0.5}\text{Co}_{0.2}\text{Mn}_{0.3}\text{O}_2$ by atomic layer deposition restrains the shuttle effect of transition metals in Li-ion capacitors *Chem. Eng. J.* **401** 126138
- [122] Ahn J, Jang E K, Yoon S, Lee S J, Sung S J, Kim D H and Cho K Y 2019 Ultrathin ZrO_2 on $\text{LiNi}_{0.5}\text{Mn}_{0.3}\text{Co}_{0.2}\text{O}_2$ electrode surface via atomic layer deposition for high-voltage operation in lithium-ion batteries *Appl. Surf. Sci.* **484** 701–9
- [123] Kong J Z, Wang S S, Tai G A, Zhu L, Wang L G, Zhai H F, Wu D, Li A D and Li H 2016 Enhanced electrochemical performance of $\text{LiNi}_{0.5}\text{Co}_{0.2}\text{Mn}_{0.3}\text{O}_2$ cathode material by ultrathin ZrO_2 coating *J. Alloys Compd.* **657** 593–600
- [124] Kong J Z, Ren C, Tai G A, Zhang X, Li A D, Wu D, Li H and Zhou F 2014 Ultrathin ZnO coating for improved electrochemical performance of $\text{LiNi}_{0.5}\text{Co}_{0.2}\text{Mn}_{0.3}\text{O}_2$ cathode material *J. Power Sources* **266** 433–9
- [125] Neudeck S, Mazilkin A, Reitz C, Hartmann P, Janek J and Brezesinski T 2019 Effect of low-temperature Al_2O_3 ALD coating on Ni-rich layered oxide composite cathode on the long-term cycling performance of lithium-ion batteries *Sci. Rep.* **9** 5328
- [126] Wang X, Cai J Y, Liu Y Q, Han X X, Ren T, Li J L, Liu Y Z and Meng X B 2021 Atomic-scale constituting stable interface for improved $\text{LiNi}_{0.6}\text{Mn}_{0.2}\text{Co}_{0.2}\text{O}_2$ cathodes of lithium-ion batteries *Nanotechnology* **32** 115401
- [127] Kong J Z, Chen Y, Cao Y Q, Wang Q Z, Li A D, Li H and Zhou F 2019 Enhanced electrochemical performance of Ni-rich $\text{LiNi}_{0.6}\text{Co}_{0.2}\text{Mn}_{0.2}\text{O}_2$ coated by molecular layer deposition derived dual-functional C- Al_2O_3 composite coating *J. Alloys Compd.* **799** 89–98
- [128] Li J W, Xiang J R, Yi G, Tang Y T, Shao H C, Liu X, Shan B and Chen R 2022 Reduction of surface residual lithium compounds for single-crystal $\text{LiNi}_{0.6}\text{Mn}_{0.2}\text{Co}_{0.2}\text{O}_2$ via Al_2O_3 atomic layer deposition and post-annealing *Coatings* **12** 84
- [129] Qin C C, Cao J L, Chen J, Dai G L, Wu T F, Chen Y B, Tang Y F, Li A D and Chen Y F 2016 Improvement of electrochemical performance of nickel rich $\text{LiNi}_{0.6}\text{Co}_{0.2}\text{Mn}_{0.2}\text{O}_2$ cathode active material by ultrathin TiO_2 coating *Dalton Trans.* **45** 9669–75
- [130] Mohanty D *et al* 2016 Modification of Ni-rich FCG NMC and NCA cathodes by atomic layer deposition: preventing surface phase transitions for high-voltage lithium-ion batteries *Sci. Rep.* **6** 26532
- [131] Zhu W C, Huang X, Liu T T, Xie Z Q, Wang Y, Tian K, Bu L M, Wang H B, Gao L J and Zhao J Q 2019 Ultrathin Al_2O_3 coating on $\text{LiNi}_{0.8}\text{Co}_{0.1}\text{Mn}_{0.1}\text{O}_2$ cathode material for enhanced cycleability at extended voltage ranges *Coatings* **9** 92
- [132] Shi Y, Xing Y J, Kim K, Yu T, Lipson A L, Dameron A and Connell J G 2021 Communication-reduction of DC resistance of Ni-rich lithium transition metal oxide cathode by atomic layer deposition *J. Electrochem. Soc.* **168** 040501
- [133] Tesfamhret Y, Younesi R and Berg E J 2022 Influence of Al_2O_3 coatings on HF induced transition metal dissolution from lithium-ion cathodes *J. Electrochem. Soc.* **169** 010530
- [134] Liu Y, Liu W B, Zhu M Y, Li Y, Li W X, Zheng F, Shen L Y, Dang M Y and Zhang J J 2021 Coating ultra-thin TiN layer onto $\text{LiNi}_{0.8}\text{Co}_{0.1}\text{Mn}_{0.1}\text{O}_2$ cathode material by atomic layer deposition for high-performance lithium-ion batteries *J. Alloys Compd.* **888** 161594
- [135] Xie J *et al* 2017 Atomic layer deposition of stable LiAlF_4 lithium ion conductive interfacial layer for stable cathode cycling *ACS Nano* **11** 7019–27
- [136] Akella S H, Taragin S, Wang Y, Aviv H, Kozen A C, Zysler M, Wang L L, Sharon D, Lee S B and Noked M 2021 Improvement of the electrochemical performance of $\text{LiNi}_{0.8}\text{Co}_{0.1}\text{Mn}_{0.1}\text{O}_2$ via atomic layer deposition of lithium-rich zirconium phosphate coatings *ACS Appl. Mater. Interfaces* **13** 61733–41
- [137] Xiao X C, Ahn D, Liu Z Y, Kim J H and Lu P 2013 Atomic layer coating to mitigate capacity fading associated with manganese dissolution in lithium ion batteries *Electrochem. Commun.* **32** 31–34
- [138] Kim J W, Kim D H, Oh D Y, Lee H, Kim J H, Lee J H and Jung Y S 2015 Surface chemistry of $\text{LiNi}_{0.5}\text{Mn}_{1.5}\text{O}_4$ particles coated by Al_2O_3 using atomic layer deposition for lithium-ion batteries *J. Power Sources* **274** 1254–62
- [139] Lee B Y, Krajewski M, Huang M K, Hasin P and Lin J Y 2021 Spinel $\text{LiNi}_{0.5}\text{Mn}_{1.5}\text{O}_4$ with ultra-thin Al_2O_3 coating for Li-ion batteries: investigation of improved cycling performance at elevated temperature *J. Solid State Electrochem.* **25** 2665–74
- [140] Xiao B W *et al* 2017 Nanoscale manipulation of spinel lithium nickel manganese oxide surface by multisite Ti occupation as high-performance cathode *Adv. Mater.* **29** 1703764
- [141] Østli E R, Ebadi M, Tesfamhret Y, Mahmoodinia M, Lacey M J, Brandell D, Svensson A M, Selbach S M and Wagner N P 2022 On the durability of protective titania coatings on high-voltage spinel cathodes *ChemSusChem* **15** e202200324
- [142] Patel R L, Palaparty S A and Liang X H 2017 Ultrathin conductive CeO_2 coating for significant improvement in electrochemical performance of $\text{LiMn}_{1.5}\text{Ni}_{0.5}\text{O}_4$ cathode materials *J. Electrochem. Soc.* **164** A6236–43
- [143] Gao Y, He X Q, Ma L, Wu T P, Park J and Liang X H 2020 Understanding cation doping achieved by atomic layer deposition for high-performance Li-Ion batteries *Electrochim. Acta* **340** 135951
- [144] Park J S, Meng X B, Elam J W, Hao S Q, Wolverton C, Kim C and Cabana J 2014 Ultrathin lithium-ion conducting coatings for increased interfacial stability in high voltage lithium-ion batteries *Chem. Mater.* **26** 3128–34
- [145] Tiurin O, Solomatin N, Auinat M and Ein-Eli Y 2020 Atomic layer deposition (ALD) of lithium fluoride (LiF) protective film on Li-ion battery $\text{LiMn}_{1.5}\text{Ni}_{0.5}\text{O}_4$ cathode powder material *J. Power Sources* **448** 227373
- [146] Deng S X *et al* 2017 New insight into atomic-scale engineering of electrode surface for long-life and safe high voltage lithium ion cathodes *Nano Energy* **38** 19–27
- [147] Deng S X *et al* 2019 Manipulation of an ionic and electronic conductive interface for highly-stable high-voltage cathodes *Nano Energy* **65** 103988
- [148] Liu J, Banis M N, Sun Q, Lushington A, Li R Y, Sham T K and Sun X L 2014 Rational design of atomic-layer-deposited LiFePO_4 as a high-performance cathode for lithium-ion batteries *Adv. Mater.* **26** 6472–7
- [149] Gao H, Cai J Y, Xu G L, Li L X, Ren Y, Meng X B, Amine K and Chen Z H 2019 Surface modification for suppressing interfacial parasitic reactions of a nickel-rich lithium-ion cathode *Chem. Mater.* **31** 2723–30
- [150] Qureshi Z A, Tariq H A, Shakoor R A, Kahraman R and AlQaradawi S 2022 Impact of coatings on the electrochemical performance of $\text{LiNi}_{0.5}\text{Mn}_{1.5}\text{O}_4$ cathode materials: a focused review *Ceram. Int.* **48** 7374–92

- [151] Gao Y, Yu H, Sandineni P, He X Q, Choudhury A, Park J and Liang X H 2021 Fe doping in $\text{LiMn}_{1.5}\text{Ni}_{0.5}\text{O}_4$ by atomic layer deposition followed by annealing: depths and occupation sites *J. Phys. Chem. C* **125** 7560–7
- [152] Zhang H, Yang Y, Ren D S, Wang L and He X M 2021 Graphite as anode materials: fundamental mechanism, recent progress and advances *Energy Storage Mater.* **36** 147–70
- [153] Jung Y S, Cavanagh A S, Riley L A, Kang S H, Dillon A C, Groner M D, George S M and Lee S H 2010 Ultrathin direct atomic layer deposition on composite electrodes for highly durable and safe Li-ion batteries *Adv. Mater.* **22** 2172–6
- [154] Wang H Y and Wang F M 2013 Electrochemical investigation of an artificial solid electrolyte interface for improving the cycle-ability of lithium ion batteries using an atomic layer deposition on a graphite electrode *J. Power Sources* **233** 1–5
- [155] Jung Y S, Lu P, Cavanagh A S, Ban C M, Kim G H, Lee S H, George S M, Harris S J and Dillon A C 2013 Unexpected improved performance of ALD coated LiCoO_2 /graphite Li-ion batteries *Adv. Energy Mater.* **3** 213–9
- [156] Zou F, Nallan H C, Dolocan A, Xie Q, Li J Y, Coffey B M, Ekerdt J G and Manthiram A 2021 Long-life $\text{LiNi}_{0.5}\text{Mn}_{1.5}\text{O}_4$ /graphite lithium-ion cells with an artificial graphite-electrolyte interface *Energy Storage Mater.* **43** 499–508
- [157] Li Y, Sun Y J, Xu G J, Lu Y, Zhang S, Xue L G, Jur J S and Zhang X W 2014 Tuning electrochemical performance of Si-based anodes for lithium-ion batteries by employing atomic layer deposition alumina coating *J. Mater. Chem. A* **2** 11417–25
- [158] Ren J G, Wu Q H, Hong G, Zhang W J, Wu H M, Amine K, Yang J B and Lee S T 2013 Silicon-graphene composite anodes for high-energy lithium batteries *Energy Technol.* **1** 77–84
- [159] Xiong S, Qian X F, Zhong Z X and Wang Y 2022 Atomic layer deposition for membrane modification, functionalization and preparation: a review *J. Membrane Sci.* **658** 120740
- [160] Wang F F, Ke X Y, Shen K, Zhu L and Yuan C 2022 A critical review on materials and fabrications of thermally stable separators for lithium-ion batteries *Adv. Mater. Technol.* **7** 2100772
- [161] Wang X R and Yushin G 2015 Chemical vapor deposition and atomic layer deposition for advanced lithium ion batteries and supercapacitors *Energy Environ. Sci.* **8** 1889–904
- [162] Chen H, Lin Q, Xu Q, Yang Y, Shao Z P and Wang Y 2014 Plasma activation and atomic layer deposition of TiO_2 on polypropylene membranes for improved performances of lithium-ion batteries *J. Membrane Sci.* **458** 217–24
- [163] Shen X *et al* 2018 Core-shell structured ceramic nonwoven separators by atomic layer deposition for safe lithium-ion batteries *Appl. Surf. Sci.* **441** 165–73
- [164] Wang W, Yuan Y, Wang J L, Zhang Y, Liao C, Mu X W, Sheng H B, Kan Y C, Song L and Hu Y 2019 Enhanced electrochemical and safety performance of lithium metal batteries enabled by the atom layer deposition on PVDF-HFP separator *ACS Appl. Energy Mater.* **2** 4167–74
- [165] Chao C-H *et al* 2021 Roll-to-roll atomic layer deposition of titania coating on polymeric separators for lithium ion batteries *J. Power Sources* **482** 228896
- [166] Liu C, Wang C C, Kei C C, Hsueh Y C and Perng T P 2009 Atomic layer deposition of platinum nanoparticles on carbon nanotubes for application in proton-exchange membrane fuel cells *Small* **5** 1535–8
- [167] Hsueh Y C, Wang C C, Kei C C, Lin Y H, Liu C and Perng T P 2012 Fabrication of catalyst by atomic layer deposition for high specific power density proton exchange membrane fuel cells *J. Catal.* **294** 63–68
- [168] Shu T, Liao S J, Hsieh C T, Roy A K, Liu Y Y, Tzou D Y and Chen W Y 2012 Fabrication of platinum electrocatalysts on carbon nanotubes using atomic layer deposition for proton exchange membrane fuel cells *Electrochim. Acta* **75** 101–7
- [169] Hsieh C T, Liu Y Y, Tzou D Y and Chen W Y 2012 Atomic layer deposition of platinum nanocatalysts onto three-dimensional carbon nanotube/graphene hybrid *J. Phys. Chem. C* **116** 26735–43
- [170] Lee W J, Bera S, Shin H C, Hong W P, Oh S J, Wan Z X and Kwon S H 2019 Uniform and size-controlled synthesis of Pt nanoparticle catalyst by fluidized bed reactor atomic layer deposition for PEMFCs *Adv. Mater. Interfaces* **6** 1901210
- [171] Lee W J, Bera S, Kim C M, Koh E K, Hong W P, Oh S J, Cho E and Kwon S H 2020 Synthesis of highly dispersed Pt nanoparticles into carbon supports by fluidized bed reactor atomic layer deposition to boost PEMFC performance *NPG Asia Mater.* **12** 40
- [172] Gan J, Zhang J K, Zhang B Y, Chen W Y, Niu D F, Qin Y, Duan X Z and Zhou X G 2020 Active sites engineering of Pt/CNT oxygen reduction catalysts by atomic layer deposition *J. Energy Chem.* **45** 59–66
- [173] Xu S C *et al* 2018 Extending the limits of Pt/C catalysts with passivation-gas-incorporated atomic layer deposition *Nat. Catal.* **624** 624–30
- [174] Liu H Y, Song Y J, Li S S, Li J, Liu Y, Jiang Y B and Guo X W 2016 Synthesis of core/shell structured $\text{Pd}_3\text{Au@Pt/C}$ with enhanced electrocatalytic activity by regioselective atomic layer deposition combined with a wet chemical method *RSC Adv.* **6** 66712–20
- [175] Zhang L *et al* 2019 Pt/Pd single-atom alloys as highly active electrochemical catalysts and the origin of enhanced activity *ACS Catal.* **9** 9350–8
- [176] Song Z X *et al* 2020 Engineering the low coordinated Pt single atom to achieve the superior electrocatalytic performance toward oxygen reduction *Small* **16** 2003096
- [177] Cheng N C, Banis M N, Liu J, Riese A, Mu S C, Li R Y, Sham T K and Sun X L 2015 Atomic scale enhancement of metal-support interactions between Pt and ZrC for highly stable electrocatalysts *Energy Environ. Sci.* **8** 1450–5
- [178] Saha S, Rodas J A C, Tan S and Li D M 2018 Performance evaluation of platinum-molybdenum carbide nanocatalysts with ultralow platinum loading on anode and cathode catalyst layers of proton exchange membrane fuel cells *J. Power Sources* **378** 742–9
- [179] Liu Y R, Hsueh Y C and Perng T P 2017 Fabrication of TiN inverse opal structure and Pt nanoparticles by atomic layer deposition for proton exchange membrane fuel cell *Int. J. Hydrog. Energy* **42** 10175–83
- [180] Tang X L, Zhang S H, Yu J, Lü C X, Chi Y Q, Sun J W, Song Y, Yuan D, Ma Z L and Zhang L X 2020 Preparation of platinum catalysts on porous titanium nitride supports by atomic layer deposition and their catalytic performance for oxygen reduction reaction *Acta Phys.-Chim. Sin.* **36** 1906070
- [181] Du Q, Wu J B and Yang H 2014 Pt@Nb-TiO₂ catalyst membranes fabricated by electrospinning and atomic layer deposition *ACS Catal.* **4** 144–51
- [182] He C, Wang X F, Sankarasubramanian S, Yadav A, Bhattacharyya K, Liang X H and Ramani V 2020 Highly durable and active Pt/Sb-doped SnO₂ oxygen reduction reaction electrocatalysts produced by atomic layer deposition *ACS Appl. Energy Mater.* **3** 5774–83

- [183] Chen J W, Li Z J, Chen Y H, Zhang J, Luo Y, Wang G and Wang R L 2020 An enhanced activity of Pt/CeO₂/CNT triple junction interface catalyst prepared by atomic layer deposition for oxygen reduction reaction *Chem. Phys. Lett.* **755** 137793
- [184] Cheng N C, Shao Y Y, Liu J and Sun X L 2016 Electrocatalysts by atomic layer deposition for fuel cell applications *Nano Energy* **29** 220–42
- [185] Yang H M, Chen Y and Qin Y 2020 Application of atomic layer deposition in fabricating high-efficiency electrocatalysts *Chin. J. Catal.* **41** 227–41
- [186] King J S, Wittstock A, Biener J, Kucheyev S O, Wang Y M, Baumann T F, Giri S K, Hamza A V, Baeumer M and Bent S F 2008 Ultralow loading Pt nanocatalysts prepared by atomic layer deposition on carbon aerogels *Nano Lett.* **8** 2405–9
- [187] Lubers A M, Muhich C L, Anderson K M and Weimer A W 2015 Mechanistic studies for depositing highly dispersed Pt nanoparticles on carbon by use of trimethyl(methylcyclopentadienyl)platinum(IV) reactions with O₂ and H₂ *J. Nanopart. Res.* **17** 179
- [188] Wang Y J, Fang B Z, Li H, Bi X T and Wang H J 2016 Progress in modified carbon support materials for Pt and Pt-alloy cathode catalysts in polymer electrolyte membrane fuel cells *Prog. Mater. Sci.* **82** 445–98
- [189] Sinniah J D, Wong W Y, Loh K S, Yunus R M and Timmiati S N 2022 Perspectives on carbon-alternative materials as Pt catalyst supports for a durable oxygen reduction reaction in proton exchange membrane fuel cells *J. Power Sources* **534** 231422
- [190] Hsu I J, Hansgen D A, McCandless B E, Willis B G and Chen J G 2011 Atomic layer deposition of Pt on tungsten monocarbide (WC) for the oxygen reduction reaction *J. Phys. Chem. C* **115** 3709–15
- [191] Saha S, Martin B, Leonard B and Li D M 2016 Probing synergetic effects between platinum nanoparticles deposited *via* atomic layer deposition and a molybdenum carbide nanotube support through surface characterization and device performance *J. Mater. Chem. A* **4** 9253–65
- [192] Chen Y G, Wang J J, Meng X B, Zhong Y, Li R Y, Sun X L, Ye S Y and Knights S 2011 Atomic layer deposition assisted Pt-SnO₂ hybrid catalysts on nitrogen-doped CNTs with enhanced electrocatalytic activities for low temperature fuel cells *Int. J. Hydrog. Energy* **36** 11085–92
- [193] Lu Q Z, Wang Z L, Tang Y T, Huang C J, Zhang A M, Liu F, Liu X, Shan B and Chen R 2022 Well-controlled Pt-CeO₂-nitrogen doped carbon triple-junction catalysts with enhanced activity and durability for the oxygen reduction reaction *Sustain. Energy Fuels* **6** 2989–95
- [194] Xu S C *et al* 2021 Direct integration of strained-Pt catalysts into proton-exchange-membrane fuel cells with atomic layer deposition *Adv. Mater.* **33** 2007885
- [195] Sairanen E, Figueiredo M C, Karinen R, Santasalo-Aarnio A, Jiang H, Sainio J, Kallio T and Lehtonen J 2014 Atomic layer deposition in the preparation of Bi-metallic, platinum-based catalysts for fuel cell applications *Appl. Catal. B* **148–149** 11–21
- [196] Lee W J, Bera S, Woo H J, Hong W, Park J Y, Oh S J and Kwon S H 2022 Atomic layer deposition enabled PtNi alloy catalysts for accelerated fuel-cell oxygen reduction activity and stability *Chem. Eng. J.* **442** 136123
- [197] Zhang L *et al* 2022 Single atom surface engineering: a new strategy to boost electrochemical activities of Pt catalysts *Nano Energy* **93** 106813
- [198] Kim Y *et al* 2022 Improving intrinsic oxygen reduction activity and stability: atomic layer deposition preparation of platinum-titanium alloy catalysts *Appl. Catal. B* **300** 120741
- [199] Dull S M, Vinogradova O, Xu S C, Koshy D M, Vullum P E, Torgersen J, Kirsch S, Viswanathan V, Jaramillo T F and Prinz F B 2022 Alloyed Pt-Zn oxygen reduction catalysts for proton exchange membrane fuel cells *ACS Appl. Energy Mater.* **5** 8282–91
- [200] Huang C J, Liu H, Tang Y T, Lu Q Z, Chu S Q, Liu X, Shan B and Chen R 2023 Constructing uniform sub-3 nm PtZn intermetallic nanocrystals via atomic layer deposition for fuel cell oxygen reduction *Appl. Catal. B* **320** 121986
- [201] Lim J, Shim J W, Kim D J, Park J S, Koo J and Shim J H 2021 Improvement of fuel cell catalyst performance through zirconia protective layer coating by atomic layer deposition *J. Power Sources* **498** 229923
- [202] Zhang L *et al* 2019 Rational design of porous structures via molecular layer deposition as an effective stabilizer for enhancing Pt ORR performance *Nano Energy* **60** 111–8
- [203] Liu Q, Ranocchiaro M and van Bokhoven J A 2022 Catalyst overcoating engineering towards high-performance electrocatalysis *Chem. Soc. Rev.* **51** 188–236
- [204] Chung S, Choun M, Jeong B, Lee J and Lee J 2016 Atomic layer deposition of ultrathin layered TiO₂ on Pt/C cathode catalyst for extended durability in polymer electrolyte fuel cells *J. Energy Chem.* **25** 258–64
- [205] McNeary W W, Linico A E, Ngo C, van Rooij S, Haussener S, Maguire M E, Pylypenko S and Weimer A W 2018 Atomic layer deposition of TiO₂ for stabilization of Pt nanoparticle oxygen reduction reaction catalysts *J. Appl. Electrochem.* **48** 973–84
- [206] Lee W J, Bera S, Woo H, Kim H G, Baek J H, Hong W, Park J Y, Oh S J and Kwon S H 2022 *In situ* engineering of a metal oxide protective layer into Pt/carbon fuel-cell catalysts by atomic layer deposition *Chem. Mater.* **34** 5949–59
- [207] Liu H, Lu Q Z, Gao Y X, Huang C J, Zhang A M, Liu F, Xu H H, Liu X, Shan B and Chen R 2023 Nitrogen doped titania stabilized Pt/C catalyst via selective atomic layer deposition for fuel cell oxygen reduction *Chem. Eng. J.* **463** 142405
- [208] Marichy C, Ercolano G, Caputo G, Willinger M G, Jones D, Rozière J, Pinna N and Cavaliere S 2016 ALD SnO₂ protective decoration enhances the durability of a Pt based electrocatalyst *J. Mater. Chem. A* **4** 969–75
- [209] McNeary W W, Zaccarine S F, Lai A, Linico A E, Pylypenko S and Weimer A W 2019 Improved durability and activity of Pt/C catalysts through atomic layer deposition of tungsten nitride and subsequent thermal treatment *Appl. Catal. B* **254** 587–93
- [210] Cheng N C, Banis M N, Liu J, Riese A, Li X, Li R Y, Ye S Y, Knights S and Sun X L 2015 Extremely stable platinum nanoparticles encapsulated in a zirconia nanocage by area-selective atomic layer deposition for the oxygen reduction reaction *Adv. Mater.* **27** 277–81
- [211] Song Z X, Wang B Q, Cheng N C, Yang L J, Banham D, Li R Y, Ye S Y and Sun X L 2017 Atomic layer deposited tantalum oxide to anchor Pt/C for a highly stable catalyst in PEMFCs *J. Mater. Chem. A* **5** 9760–7
- [212] Hussain S, Erikson H, Kongi N, Tarre A, Ritslaid P, Rähn M, Matisen L, Merisalu M, Sammelselg V and Tammeveski K 2018 Pt nanoparticles sputter-deposited on TiO₂/MWCNT composites prepared by atomic layer deposition: improved electrocatalytic activity towards the oxygen reduction reaction and durability in acid media *Int. J. Hydrog. Energy* **43** 4967–77
- [213] Hussain S, Erikson H, Kongi N, Tarre A, Ritslaid P, Kook M, Rähn M, Merisalu M, Sammelselg V and Tammeveski K 2019 Improved ORR activity and long-term durability of Pt nanoparticles deposited on TiO₂-decorated multiwall carbon nanotubes *J. Electrochem. Soc.* **166** F1284–91

- [214] Song Z X *et al* 2018 Origin of achieving the enhanced activity and stability of Pt electrocatalysts with strong metal-support interactions via atomic layer deposition *Nano Energy* **53** 716–25
- [215] Sabarirajan D C, George T Y, Vlahakis J, White R D and Zenyuk I V 2019 Atomic layer deposition of Pt nanoelectrode array for polymer electrolyte fuel cells *J. Electrochem. Soc.* **166** F3081–8
- [216] Atwa M, Li X A, Wang Z X, Dull S, Xu S C, Tong X, Tang R, Nishihara H, Prinzege F and Birss V 2021 Scalable nanoporous carbon films allow line-of-sight 3D atomic layer deposition of Pt: towards a new generation catalyst layer for PEM fuel cells *Mater. Horiz.* **8** 2451–62
- [217] Dull S M *et al* 2021 Bottom-Up fabrication of oxygen reduction electrodes with atomic layer deposition for high-power-density PEMFCs *Cell Rep. Phys. Sci.* **2** 100297
- [218] Shu T, Dang D, Xu D W, Chen R, Liao S J, Hsieh C T, Su A, Song H Y and Du L 2015 High-performance MEA prepared by direct deposition of platinum on the gas diffusion layer using an atomic layer deposition technique *Electrochim. Acta* **177** 168–73
- [219] Song Z X *et al* 2019 Ultralow loading and high-performing Pt catalyst for a polymer electrolyte membrane fuel cell anode achieved by atomic layer deposition *ACS Catal.* **9** 5365–74
- [220] Lubers A M, McNeary W W, Ludlow D J, Drake A W, Faust M, Maguire M E, Kodas M U, Seipenbusch M and Weimer A W 2017 Proton exchange membrane fuel cell flooding caused by residual functional groups after platinum atomic layer deposition *Electrochim. Acta* **237** 192–8
- [221] McNeary W W, Linico A E and Weimer A W 2020 Water management implications for ALD-modified polymer electrolyte membrane fuel cell catalysts *J. Nanopart. Res.* **22** 185
- [222] Choun M, Chung S, Jeon H, Uhm S and Lee J 2012 Atomic-layer-deposited TiO₂ on cathode gas diffusion layer for low humidity operation in hydrogen fuel cells *Electrochem. Commun.* **24** 108–11
- [223] Lim I S, Kang B, Park J Y and Kim M S 2021 Performance improvement of polymer electrolyte membrane fuel cell by gas diffusion layer with atomic-layer-deposited HfO₂ on microporous layer *Energy Convers. Manage.* **236** 114070
- [224] Toikkanen O, Nisula M, Pohjalainen E, Hietala S, Havansi H, Ruotsalainen J, Halttunen S, Karppinen M and Kallio T 2015 Al₂O₃ coating grown on Nafion membranes by atomic layer deposition *J. Membrane Sci.* **495** 101–9
- [225] Libera J A, Elam J W and Pellin M J 2008 Conformal ZnO coatings on high surface area silica gel using atomic layer deposition *Thin Solid Films* **516** 6158–66
- [226] Stempel V E, d'Alnoncourt R N, Driess M and Rosowski F 2017 Atomic layer deposition on porous powders with *in situ* gravimetric monitoring in a modular fixed bed reactor setup *Rev. Sci. Instrum.* **88** 074102
- [227] Voigt P, Haimi E, Lahtinen J, Cheah Y W, Mäkelä E, Viinikainen T and Puurunen R L 2019 Nickel supported on mesoporous zirconium oxide by atomic layer deposition: initial fixed-bed reactor study *Top. Catal.* **62** 611–20
- [228] Hakim L F, Blackson J, George S M and Weimer A W 2005 Nanocoating individual silica nanoparticles by atomic layer deposition in a fluidized bed reactor *Chem. Vap. Depos.* **11** 420–5
- [229] McCormick J A, Cloutier B L, Weimer A W and George S M 2007 Rotary reactor for atomic layer deposition on large quantities of nanoparticles *J. Vac. Sci. Technol. A* **25** 67–74
- [230] Park S W, Kim J W, Choi H J and Shim J H 2014 Vibration atomic layer deposition for conformal nanoparticle coating *J. Vac. Sci. Technol. A* **32** 01A115
- [231] Lu Z, Yanguas-Gil A, Kang D, Darapaneni P, Mane A U, Marshall C L and Elam J W 2022 Scalable synthesis of supported catalysts using fluidized bed atomic layer deposition *J. Vac. Sci. Technol. A* **40** 042404
- [232] Coile M W, Young M J, Libera J A, Mane A U and Elam J W 2020 High-capacity rotary drum for atomic layer deposition onto powders and small mechanical parts in a hot-walled viscous flow reactor *J. Vac. Sci. Technol. A* **38** 052403
- [233] Li J G, Hui L F, Zhang W L, Lu J, Yang Y J and Feng H 2021 Scalable production of ultra small TiO₂ nano crystal/activated carbon composites by atomic layer deposition for efficient removal of organic pollutants *Adv. Powder Technol.* **32** 728–39
- [234] Lee W J, Kwon O, Huang R J, Lin C, Gorte R J and Vohs J M 2022 Flexible atomic layer deposition system for coating porous materials *J. Vac. Sci. Technol. A* **40** 032401
- [235] Duan C L, Liu X, Shan B and Chen R 2015 Fluidized bed coupled rotary reactor for nanoparticles coating via atomic layer deposition *Rev. Sci. Instrum.* **86** 075101
- [236] Li Z S, Xiang J R, Liu X, Li X B, Li L J, Shan B and Chen R 2022 A combined multiscale modeling and experimental study on surface modification of high-volume micro-nanoparticles with atomic accuracy *Int. J. Extreme Manuf.* **4** 025101
- [237] van Ommen J R, Kooijman D, de Niet M, Talebi M and Goulas A 2015 Continuous production of nanostructured particles using spatial atomic layer deposition *J. Vac. Sci. Technol. A* **33** 021513
- [238] Hartig J, Howard H C, Stelmach T J and Weimer A W 2021 DEM modeling of fine powder convection in a continuous vibrating bed reactor *Powder Technol.* **386** 209–20
- [239] Poodt P, Cameron D C, Dickey E, George S M, Kuznetsov V, Parsons G N, Roozeboom F, Sundaram G and Vermeer A 2012 Spatial atomic layer deposition: a route towards further industrialization of atomic layer deposition *J. Vac. Sci. Technol. A* **30** 010802
- [240] Muñoz-Rojas D, Maindron T, Esteve A, Piallat F, Kools J C S and Decams J M 2019 Speeding up the unique assets of atomic layer deposition *Mater. Today Chem.* **12** 96–120
- [241] Sharma K, Routkevitch D, Varaksa N and George S M 2016 Spatial atomic layer deposition on flexible porous substrates: ZnO on anodic aluminum oxide films and Al₂O₃ on Li ion battery electrodes *J. Vac. Sci. Technol. A* **34** 01A146
- [242] Yersak A S, Sharma K, Wallas J M, Dameron A A, Li X, Yang Y, Hurst K E, Ban C, Tenent R C and George S M 2018 Spatial atomic layer deposition for coating flexible porous Li-ion battery electrodes *J. Vac. Sci. Technol. A* **36** 01A123